CANADIAN THESES ON MICROFICHE

I.S.B.N.

THESES CANADIENNES SUR MICROFICHE

National Library of Canada
Collections Development Branch

Canadian Theses on
Microfiche Service

Ottawa, Canada
K1A 0N4

Bibliothèque nationale du Canada
Direction du développement des collections

Service des thèses canadiennes
sur microfiche

NOTICE

The quality of this microfiche is heavily dependent upon the quality of the original thesis submitted for microfilming. Every effort has been made to ensure the highest quality of reproduction possible.

If pages are missing, contact the university which granted the degree.

Some pages may have indistinct print especially if the original pages were typed with a poor typewriter ribbon or if the university sent us a poor photocopy.

Previously copyrighted materials (journal articles, published tests, etc.) are not filmed.

Reproduction in full or in part of this film is governed by the Canadian Copyright Act, R.S.C. 1970, c. C-30. Please read the authorization forms which accompany this thesis.

THIS DISSERTATION
HAS BEEN MICROFILMED
EXACTLY AS RECEIVED

AVIS

La qualité de cette microfiche dépend grandement de la qualité de la thèse soumise au microfilmage. Nous avons tout fait pour assurer une qualité supérieure de reproduction.

S'il manque des pages, veuillez communiquer avec l'université qui a conféré le grade.

La qualité d'impression de certaines pages peut laisser à désirer, surtout si les pages originales ont été dactylographiées à l'aide d'un ruban usé ou si l'université nous a fait parvenir une photocopie de mauvaise qualité.

Les documents qui font déjà l'objet d'un droit d'auteur (articles de revue, examens publiés, etc.) ne sont pas microfilmés.

La reproduction, même partielle, de ce microfilm est soumise à la Loi canadienne sur le droit d'auteur, SRC 1970, c. C-30. Veuillez prendre connaissance des formules d'autorisation qui accompagnent cette thèse.

LA THÈSE A ÉTÉ
MICROFILMÉE TELLE QUE
NOUS L'AVONS REÇUE

NL-339 (r. 82/08)

Canada

A SEARCH FOR QUANTUM CHANGES IN THE AXIAL FLUX AS A TRANSPORT CURRENT IS VARIED IN A TYPE II SUPERCONDUCTOR IN A LONGITUDINAL MAGNETIC FIELD

© James E. Gort

Thesis submitted to the School of Graduate Studies of the University of Ottawa in partial fulfillment of the requirements for the degree

Master of Science

1982

UNIVERSITÉ D'OTTAWA
UNIVERSITY OF OTTAWA

ACKNOWLEDGEMENTS

I would like to express my gratitude to my thesis supervisor, Professor Marcel LeBlanc, for his suggestion of this avenue of research and for his invaluable guidance in performing the experiments and interpreting the results. His keen interest encouraged me to complete this thesis at a time of numerous other priorities.

I am also indebted to the advice received from Professor Gilles Lamarche in all phases of the SQUID operation and analysis. He has generously allowed me to share his laboratory and equipment and to profit from his experience and insight.

The financial support obtained from the National Research Council of Canada is also acknowledged.

ABSTRACT

This thesis describes a search for quantum changes in the axial flux of a superconductor. When a type II cylindrical superconductor is placed in a longitudinal magnetic field and its transport current is slowly varied, helical fluxlines at the surface of the cylinder migrate into (or from) the sample, causing a change in the axial magnetic flux threading the sample. The experiments described here investigate those flux changes at the quantum level for various magnetic histories of the sample. The experimental arrangements used in exploring these small flux changes are also described in considerable detail.

Although these experiments apparently did not detect a single flux quantum, they did verify known magnetic properties at the quantum level and an unusual magnetic regime was investigated.

LIST OF ILLUSTRATIONS

TABLE OF CONTENTS

I. INTRODUCTION TO THE MAGNETIC PROPERTIES OF TYPE II SUPERCONDUCTORS

A. Introduction

A brief acquaintance with the magnetic properties of type II Superconductors serves two purposes. First, it puts the goal and approach of this research in the light of historical context. Second, it permits a qualitative appreciation of models which attempt to explain certain observed phenomena reported here.

This chapter will concentrate on properties which are relevant to the understanding and interpretation of the experimental work described in subsequent chapters. In all cases, emphasis will be placed on the cylindrical geometry and applied magnetic fields along the axis of the cylinder to facilate relating theory to these experiments. No attempt is made to describe or apply the detailed microscopic theory to the treatment of properties of type II superconductors. Indeed, such an application of microscopic theory to predict observed phenomena has only been successful for very special cases of geometry and magnetic field arrangements (1,2,3) due to formidable theoretical obstacles. Rather, the phenomenological approach of Ginzburg-Landau is adopted which, together with the equations of London and Maxwell, give good insight into the physical processes associated with type II superconductors. Certain models of those physical processes which attempt to predict microscopic observations are also briefly described to complete the theoretical foundation.

B. Magnetic Behaviour

One of the principal observed features of a type II superconductor is its magnetization curve, a typical example of which is shown in Figure 1. When a magnetic field, H_z, is applied to a superconducting sample and its magnetization, M_z, is measured (by means of pick-up coils or a SQUID magnetometer to be discussed later) along the same direction, two critical fields, H_{c_1} and H_{c_2}, may be defined. In the regime below H_{c_1}, the magnetization curve is linear of unity slope or, in cgs units,

$$-4\pi M_z = H_z.$$

If we compare this equation with the relationship

$$\overline{B} = \overline{H} + 4\pi\overline{M},$$

it is evident that $\overline{B} = 0$, i.e., perfect diamagnetism, exists within the sample for $H_z < H_{c_1}$. This condition is true regardless of the previous history of the sample. For instance, if the sample were cooled through its superconducting transition temperature in the presence of any field $H < H_{c_1}$, all magnetic flux threading the sample would be expelled at transition. The observed magnetization would abruptly change from zero at $T > T_c$ to a point on the linear magnetization curve at $T \leq T_c$.

Another feature of the magnetization curve is its change in slope when $H_z = H_{c_1}$. As the applied field is increased past H_{c_1}, magnetic flux begins to penetrate the superconductor, giving rise to a $B_z(x)$ profile within the sample and the so-called "mixed state". Various critical state models have been devised to relate these flux gradients to certain forces acting within the sample in an effort to explain observed effects. It should be remembered that those flux gradients are inaccessible to measure-

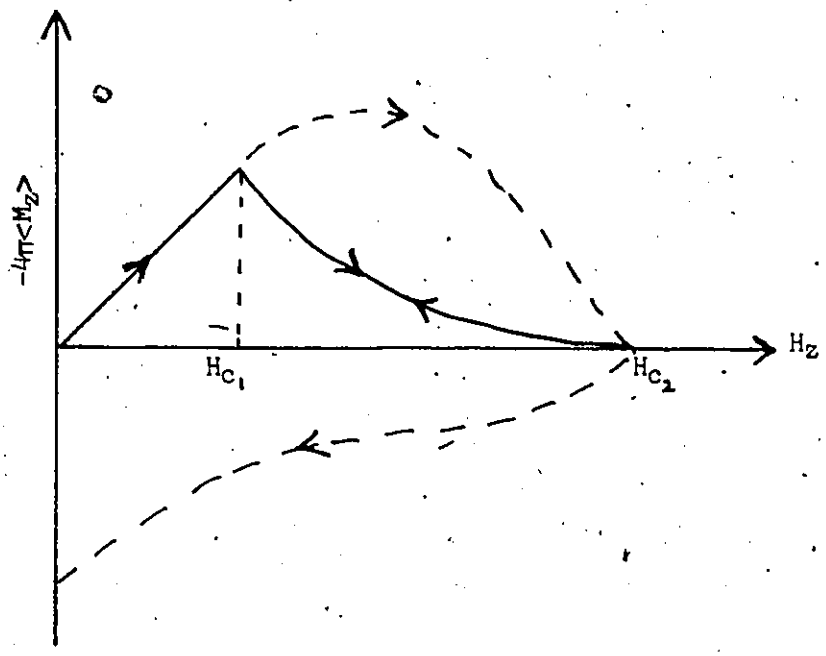

Fig. 1 Ideal or reversible (solid line) and non-ideal or irreversible (dashed line) magnetization curve of a type II superconductor.

ment; the phenomena directly observable are the bulk magnetization as described here and the electric current density through voltage probes on the surface of the sample.

As the applied field is increased, more flux penetrates the sample until $H_z = H_{c_2}$, at which point flux threads the entire sample and the bulk becomes completely normal. However, superconductivity may persist in a thin surface sheath until a higher critical field, H_{c_3}, resulting in a small tail on the magnetization curve. In some situations the surface of the sample may also have a significant influence on its magnetic behaviour at applied fields below H_{c_2}.

Another feature evident from an analysis of the magnetization curve is the sample's hysteretic behaviour. In an "ideal" type II superconductor the magnetic behaviour is completely reversible, that is, when the applied field is reduced or cycled in the regime $0 < H_z < H_{c_2}$, the magnetization curve is retraced upon itself. With a non-ideal or irreversible type II (such as examined in the experiments reported here) the curve is not retraced and the magnetization is no longer only a function of applied field but also of the sample's magnetic history. As illustrated in Figure 1, an irreversible sample cycled back to zero applied field will have a net residual magnetization, even though it may have begun the cycle with no magnetization. The mechanics and implications of irreversible behaviour is a large component of the remainder of this chapter.

It should be noted in passing that cycling in the regime $0 < H_z < H_{c_1}$ is completely reversible even in non-ideal superconductors, provided H_{c_1} has not been exceeded. This, however, is of no interest for an understanding of experiments described later.

C. The Mixed State and Flux Vortices

The magnetization curve shows that magnetic flux obviously penetrates the interior of a type II superconductor in an applied field H_z between H_{c_1} and H_{c_2}. But how does this penetration occur? London (4) showed in 1935 that the boundary between superconducting and normal regions is not infinitely sharp, but rather magnetic flux at the surface, B(0), of a sample decays exponentially with distance, x, into the sample as

$$B(x) = B(0)\exp(-x/\lambda)$$

where λ defines a characteristic penetration depth, typically of the order of 10^{-6}cm. Such a small penetration depth, however, has a negligibly small effect on the magnetization curve, leading early workers to search for other mechanisms of flux penetration.

Pippard (5) in 1953 introduced the concept of a coherence length, ξ, which defined the way in which two interpenetrating electronic fluids, each of a different degree of order, are related. He reasoned that at a superconducting-normal boundary, the order, and hence the density of "superelectrons" (n_s), was not discontinuous, but exponentially varies with a characteristic length ξ, typically of the order of 10^{-4}cm for a pure superconductor (reduced in the presence of impurities).

Abrikosov (6) deduced that energy considerations due to the magnetic flux contribution (penetration depth, λ) and the electron ordering contribution (coherence length, ξ) have a prime role to play in explaining macroscopic flux penetration in the mixed state. Figure 2 illustrates the energy-related implications. He reasoned that if $\xi < \lambda\sqrt{2}$, a negative surface energy results at the normal-superconducting boundary. The sample therefore finds it energet-

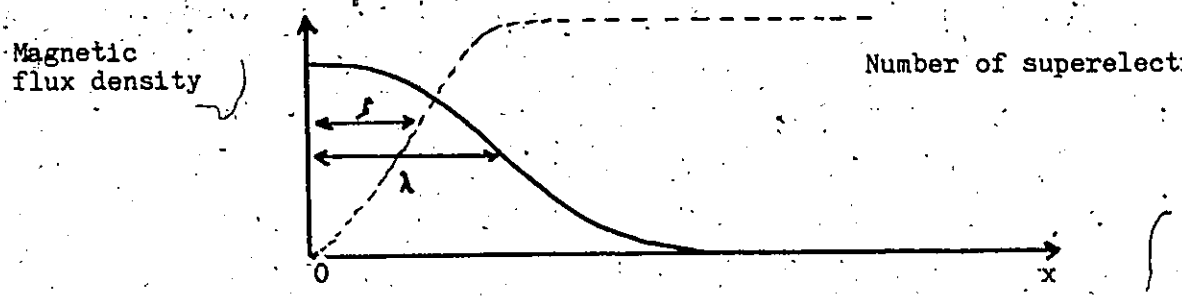

Penetration depth, λ, and coherence length, ξ, at superconducting-normal boundary.

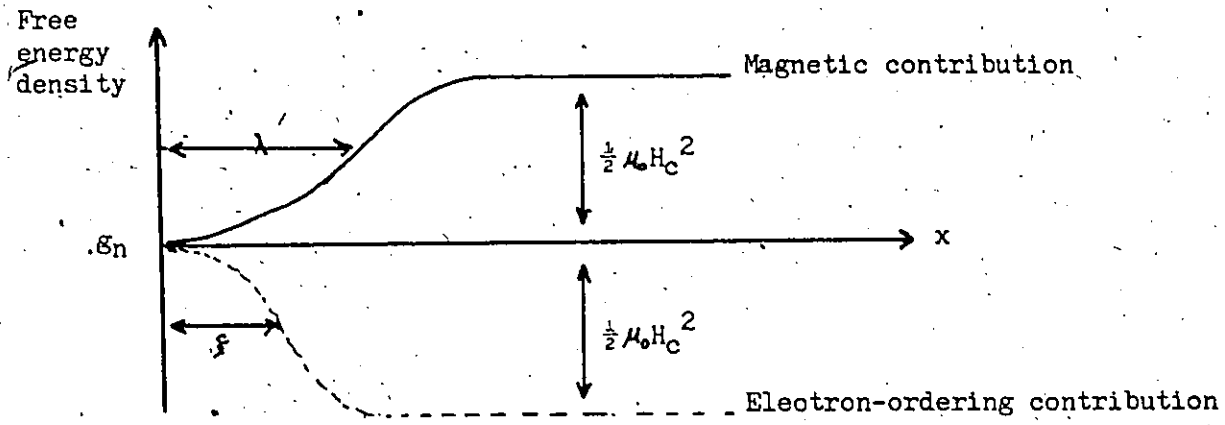

Contributions to free energy.

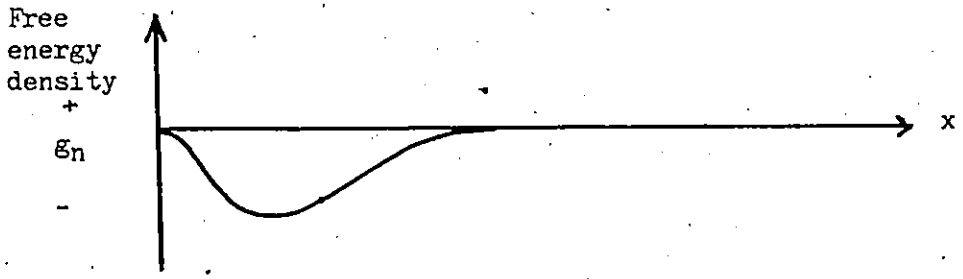

Total free energy (sum of both contributions)

Fig. 2 Negative surface energy in a type II superconductor.

ically favourable to divide into small superconducting regions interspersed with normal regions, producing a filamentary structure, as shown in Figure 3. He further reasoned that, in this filamentary picture, magnetic flux can indeed penetrate into the bulk of a type II superconductor in the form of quantized flux filaments, or vortices. Each vortex consists of a normal core surrounded by circulating currents enclosing one quantum of flux, $\Phi_o = hc/2e = 2 \times 10^{-7}$ Gauss-cm^2.

Rocher and Renard (7) however, have raised the theoretical possibility that, in certain instances, several-quanta flux lines may be more stable. Experimental evidence for the existence of flux vortices may now be considered conclusive (8, 9, 10, 11).

The movement of these vortices give rise to the magnetic properties of type II superconductors, and that movement will be explored briefly in a subsequent section. Suffice it to say for now that vortices will move due to the action of various forces, including that due to their mutual repulsion, thermal gradients, transport currents, local magnetic field, and "pinning" (which immobilizes vortices due to certain impurities and imperfections). Pinning also is apparently the cause of magnetic irreversibility, discussed in more detail in the following section.

D. Magnetic Irreversibility and Flux Flow

Irreversible magnetic behaviour is attributed to the fact that the normal cores which thread the superconductor in the mixed state are influenced by local energy minima near imperfections in the sample. the vortex therefore finds its energetically favourable to remain in the

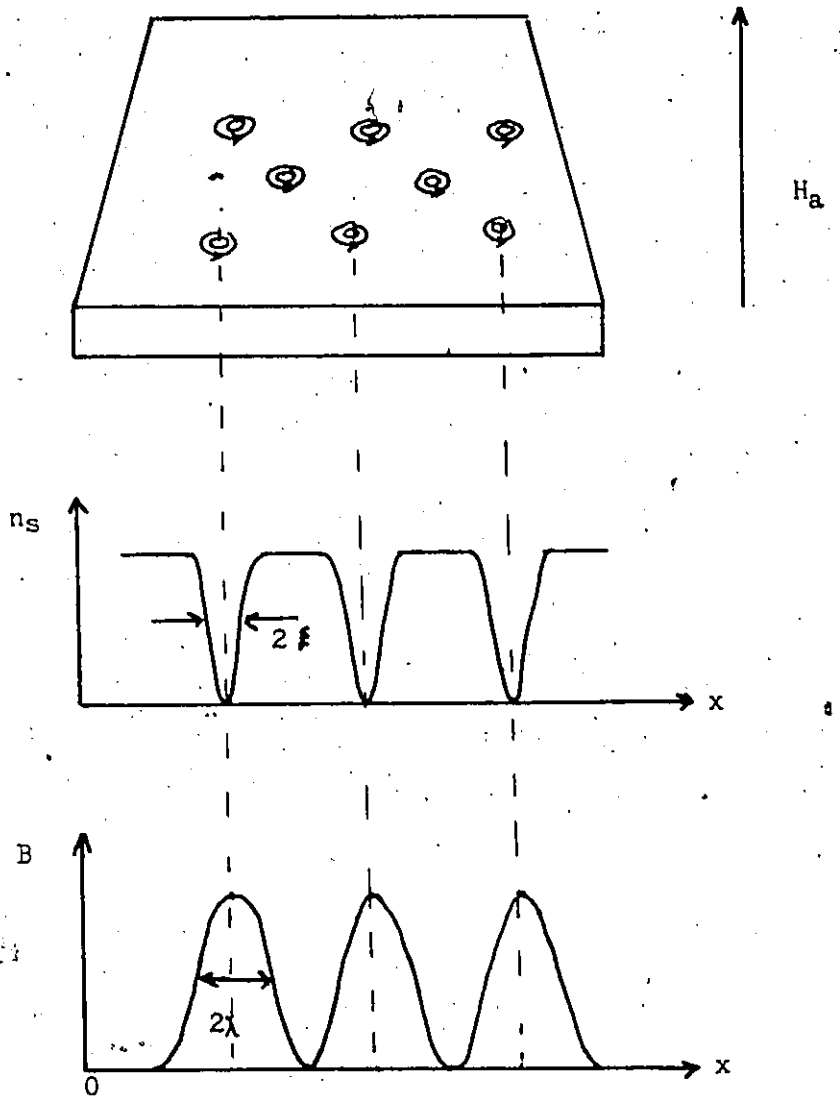

Fig. 3 Filamentary structure of a type II superconductor in an applied magnetic field $H_a > H_{c_1}$. Also shown is the variation of the number of superelectrons, n_s, with distance, x, and the variation of magnetic flux density, B, with x.

vicinity of the imperfection, being constrained from moving freely under the influence of Lorentz

and other forces, until a sufficiently strong force exceeds the "pinning" force. Thus, when an axial magnetic field surrounding a type II superconductor is increased to a field $H_{c_1} < H_z < H_{c_2}$ and then lowered, there is a hysteresis since some flux is trapped in the sample by pinning of vortices.

Suppose such an irreversible cylindrical superconductor of cross-sectional area A is placed in an axial magnetic field B_z and carries a current, i. Due to the induced azimuthal field at the surface B_ϕ, resulting from the current flow, the resultant field (vector sum) in the superconductor will be directed at some angle $\theta(r)$ to the current direction, where θ is a function of radial distance from the axis. If the average current density $J = i/A$, the Lorentz force per unit length of each vortex is

$$F_L = JB(r)\sin\theta(r)/n$$

where n = number of vortices per unit area.

If the current density J produces a Lorentz force F_L less than the average pinning force per unit length of core, F_p, the core lattice will be stable.

Not every core, of course, is directly pinned to an imperfection in the material. The interaction between vortices is sufficient, however, to stabilize the whole lattice if only relatively few cores are pinned. It is therefore appropriate to talk of the <u>average</u> pinning force per core, since it is that quantity which may be compared to the Lorentz force (which works on <u>every</u> core).

Pinned vortices may be set in motion when $F_L > F_p$. The transport cur-

rent is therefore doing work on the cores, which are moving through the sample and being opposed by a viscous force. Since their motion is impeded, a voltage drop is noted along the sample, giving rise to the "flux flow" state. This flow resistivity has been observed when the transport current exceeds a certain critical current in the experiments reported in a later chapter, and sample magnetization was also monitored in this regime. It was previously found (12) and verified here that two clearly distinguishable regimes can exist. One regime shows magnetically irreversible behaviour and no potential difference along the sample while the other displays a flux flow resistance but the magnetic moment is a reversible function of applied current and field.

In summary, when a magnetically reversible type II superconductor is placed in a uniform magnetic field, an Abrikosov fluxline lattice of uniform density is established in the bulk. If a transport current parallel to the field is applied, a Lorentz force free (12, 13, 14) flux and current structure is established; that is, the local current density $\bar{J}$ and field $\bar{B}$ are parallel everywhere.

When an irreversible superconductor is placed in a uniform field, a non-uniform fluxline lattice is established. The distribution of flux depends on the magnetic history of the sample and the nature of the pinning centres. Models, such as the Bean - London critical state model have been used to approximate the flux distribution and therefore predict the magnetic behaviour of the sample.

E. Flux pinning

It has been observed that the pinning force F_p increases initially as the internal magnetic field B is increased, sometimes stated as $F_p \propto \alpha(T)B^n$. The pinning dependence on B is probably due to the fact that the number of vortices increase with B and it is mainly the interation of vortex cores with the pinning sites that causes the vortex lattice to be pinned. It should be noted that the pinning force depends on the total magnetic field $B = \sqrt{B_\perp^2 + B_\parallel^2}$, since this quantity determines the vortex core density. The Lorentz force, however, depends on $B_\perp$, the component of B perpendicular to the electric current. Thus, the critical state equation $F_L = F_p$ may be expressed as

$$j_c B_\perp = \alpha_n (B_\perp^2 + B_\parallel^2)^{n/2}.$$

Therefore, for $n > 0$, j_c may be increased by increasing the component of magnetic field parallel to the current, $B_\parallel$. It follows that the critial current density may be enhanced in type II superconductors in the presence of an axial magnetic field. This prediction is experimentally verified in a subsequent chapter.

The critical state concept (i.e., $F_L = F_p$) implies that a maximum flux gradient may exist in the bulk, determined by the mutual repulsion of vortices and the strength of the pinning. If the applied external field is adjusted, the internal flux gradient may temporarily exceed the maximum value, but a redistribution of vortex cores occurs on a relatively short time scale. That is, a flux wavefront propagates through the bulk with a characteristic "magnetic diffusivity". Pinning prevents a homogeneous distribution of vortices in these irreversible samples. Flux

creep (18) may occur in some samples, increasing the time scale for vortex redistribution. Thus, the critical state is usually defined only for cases of negligible flux creep.

Flux jumps may also occur, that is, a macroscopic flux change caused by the sudden movement of many vortices. Since each pinned vortex will be immobilized until an applied force causes its movement, the vortex may be released from its pinning site and suddenly move to a distant site. Due to the vortex interactions, an entire section of the flux lattice may suddenly shift, causing an apparent discontinuity in the observed magnetization. Since flux movement causes local heating, a large flux jump may induce sufficient heating that the sample may be driven normal. These catastrophic flux jumps have been studied by several workers (16, 17).

F. Surface layer effects

Although the critical current of a type II superconductor falls rapidly as the applied field exceeds H_{c_2}, some samples can nevertheless carry a small resistanceless current (experimentally reported in a later chapter) to a higher field, H_{c_3}. The value of H_{c_3} depends on the angle which the applied field makes with the surface, reaching a maximum for an applied parallel field, when $H_{c_3} \approx 1.7\ H_{c_2}$.

A theoretical explanation was advanced by St. James and De Gennes (18), who showed that superconductivity can exist close to the surface (a few hundred $\mathring{A}$ deep) even when the bulk has been driven normal. It has since been shown that such a surface sheath exists for all fields $0 < H < H_{c_2}$

and may play an important part in determining magnetic and critical current behaviour of type II superconductors.

G. Response to transport current in a longitudinal field

a. Critical current dependence on a longitudinal field

A well-known observed phenomenon in a type II cylindrical sample in a longitudinal magnetic field is the increase in the critical transport current due to the axial magnetic induction, B_z. This phenomenon is easily understood by the critical state concept, which requires that the total Lorentz force, F_L, on a vortex be equal to its pinning force, F_p (in the critical steady state, in the absence of flux flow). The "outward" force on a vortex, $F_L(o)$, considered to be a consequence of the axial flux and resulting in a paramagnetic azimuthal current, J_θ, can be written:

$$F_L(o) = J_\theta B_z.$$

The "inward" force on a vortex, $F_L(i)$, considered to be a consequence of the transport current density, J_z, and generating an azimuthal magnetic induction, B_θ, can be written:

$$F_L(i) = J_z B_\theta.$$

The net Lorentz force is less than or equal to the pinning force in the steady state, or

$$\left|F_L(o) - F_L(i)\right| \leq \left|F_p\right|$$

It is obvious that for a constant pinning force density, $F_L(i)$ may be greater when $F_L(o)$ is greater. Therefore, the magnetic field causes an increase in the critical J_z allowed before the pinning force is exceeded and flux flow occurs.

Another contribution to the observed increase in the critical current density in the presence of an axial magnetic field is the pinning force dependence on the total field. Since initially $F_p \propto \alpha_n B^n$, B_z results in a higher F_p and hence a higher critical J_z is allowed. In the presence of higher fields, however, the pinning force decreases as $F_p \propto (1 - (B/B_{c_2})^n)$, becoming nil at $B = B_{c_2}$. This contribution to the increase in the critical current density is therefore only important when $B \ll B_{c_2}$; as B approaches B_{c_2}, the critical J_z is reduced due to the reduced pinning.

b. Current flow and magnetic moment of a sample in a longitudinal field

When a transport current is applied to a sample in a longitudinal field, a complex structure of helical fluxlines is established, resulting from the interaction of the local magnetic field within the superconductor based on its magnetic history, the induced local field from the transport current, and the three-dimensional pinning force dependence on the magnitude and direction of the local field. It has, in fact, been experimentally established that helical fluxlines result even in the case of axial current flow in no applied field (20).

Magnetization of a sample carrying a transport current in an axial field has been studied (21) and found to cycle between paramagnetic and diamagnetic as the current was impressed and removed. A simple model was advanced (21) which requires that the transport current and induced currents flow in helical paths and that i) the net critical Lorentz force density is constant in the sample and directed inward, and ii) the existing flux configuration is preserved consistent with the change in the applied current.

Walmsley (14) has studied the magnetization of samples as a transport current is varied in a constant axial field, the results of which of which are shown in Figure 4. Both the diamagnetic and paramagnetic regimes are shown; in all cases, an increase in the transport current results in a decrease in diamagnetism or an increase in paramagnetism.

An interesting phenomenon reported by Walmsley (14) and also investigated by Nicholson and Sikora (22) is the reversible flux flow resistive state as the current reaches a critical value, also shown in Figure 4. This regime was also investigated in the experiments described in section 4 of this thesis.

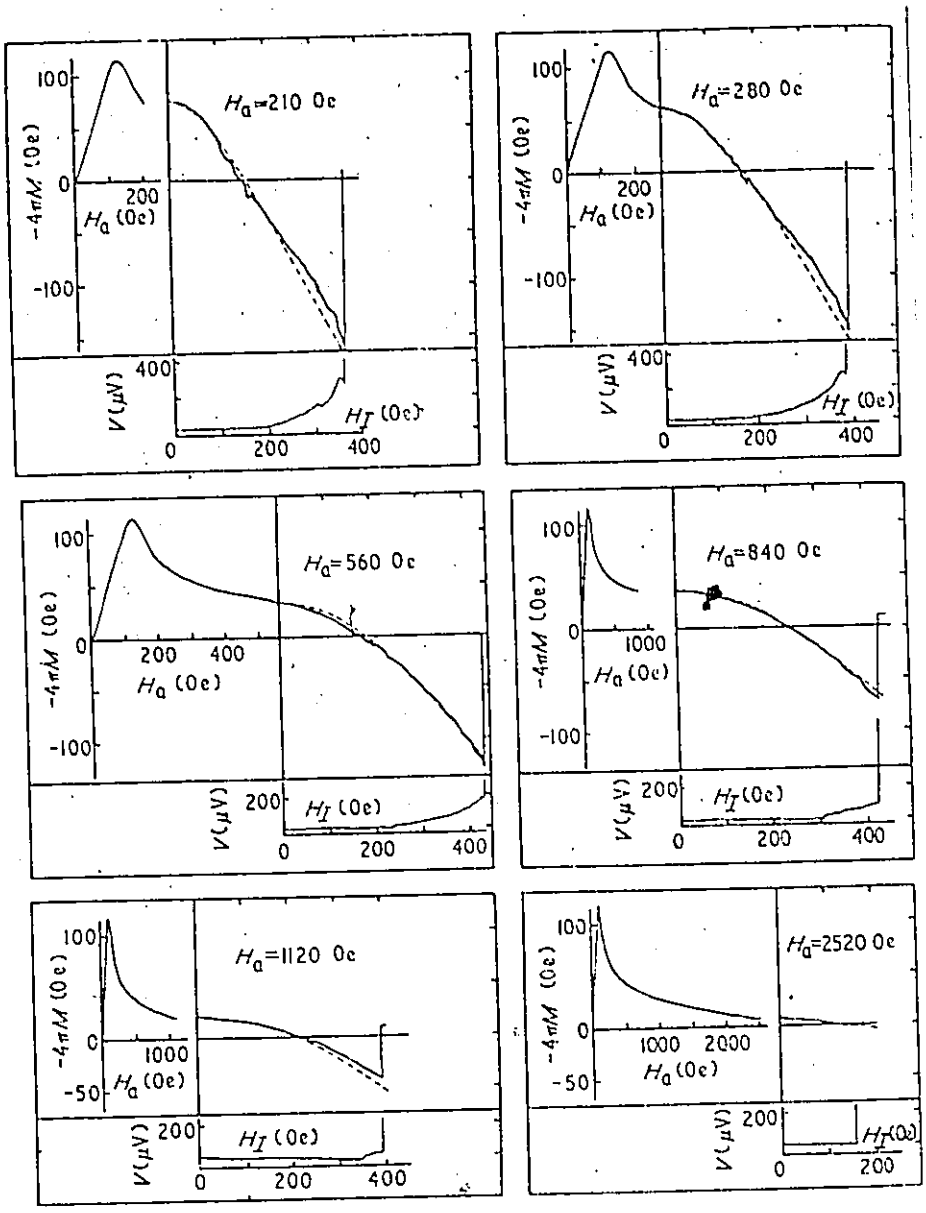

Fig. 4 Magnetization as a function of applied field H_a and current. The axial potential drop is also plotted as a function of current. H_a is held fixed while current increases. From Walmsley (14).

II. SQUIDS: THEORY AND APPLICATION

A. Introduction

SQUIDs (Superconduction QUantum Interference Devices) are magnetic flux sensors which exploit the concept of flux quantization and the effect predicted by Josephson (23) to provide extreme magnetic sensitivity (to the level of a fraction of a flux quantum) and excellent noise performance. In fact the sensitivity is only limited by the noise either within the SQUID, its electronics, or the external world, and these will be discussed in more detail below.

Several types of SQUIDs have been developed and each may be particularly suited for a variety of applications. There are both single and double junction SQUIDs, the junction of which may comprise one of a number of weak link configurations. In addition, the SQUID may be operated in either the RF or dc mode. The observed characteristics of the SQUID is therefore a function of both its weak link(s) and operational mode.

This chapter will be concerned with the theory and application of the specific SQUID used in the experiments described later, that is, a symmetrical single-point-contact RF SQUID. Moreover, the application of determining a small change in magnetization of a cylindrical sample will be stressed, including the use of a flux transformer to couple an external flux change to a flux change within the SQUID.

B. Theory

a. Flux quantization

The concept of magnetic flux quantization plays an important part in understanding the principle of operation of the SQUID, since the heart of the SQUID, a ring containing a Josephson junction weak link, permits only an integral number of flux quanta to thread the ring. It is therefore appropriate to briefly discuss flux quantization and the Josephson effect (in its application to the RF SQUID) prior to any discussion of the application of the SQUID to magnetization measurements.

London (24) first proposed that magnetic flux linking a superconductor was quantized in an integral number of "flux quanta", or ϕ_o. He reasoned that a macroscopic wavefunction for the superelectrons, ψ, may be characterized by a phase factor, θ, and written

$$\psi = \exp i\theta$$

where $$\theta = \frac{\bar{P} \cdot \bar{r}}{\hbar}$$

and $\bar{P}$ = momentum of superelectrons.

Now, assume that a current is applied to the superconductor in the presence of a magnetic field. Then,

$$\bar{P} = m^*\bar{v} + e^*\bar{A}$$

where m^* = effective mass

$\bar{v}$ = velocity of superelectrons

e^* = effective charge of superelectrons

$\bar{A}$ = magnetic vector potential.

Of course,

$$\bar{v} = \bar{J}/\rho e^*$$

where $\bar{J}$ = supercurrent density

ρ = density of superelectrons (pairs)

The phase difference around any closed path within the superconductor is due to the phase contributions of both the supercurrent and the vector potential, such that

$$\oint d\theta = \frac{m^*}{\rho e^* \hbar} \oint \bar{J} \cdot d\bar{l} + \frac{e^*}{\hbar} \oint \bar{A} \cdot d\bar{l}$$

Since ψ is a single-valued wavefunction, the phase change $\Delta\theta$ around any closed path must be

$$\oint d\theta = 2\pi n$$

where n = any integer.

Therefore,

$$\rho \frac{m^*}{e^{*2}} \oint \bar{J} \cdot d\bar{l} + \oint \bar{A} \cdot d\bar{l} = \frac{2n\pi\hbar}{e^*}$$

Since the left hand side of this equation is obviously a constant and in units of magnetic flux, the term "fluxoid" or "flux quantum" was applied to the lowest quantum level ($n = 1$) of magnetic flux threading any closed path in a superconductor. London computed the value of Φ_o to be 4×10^{-7} G - cm^2, but subsequent experimental observations (25, 26) yielded a value only one-half as large. We now understand that Cooper pairs carry a charge of twice that of normal electrons, so that $e^* = 2e$.

b. The Josephson effect

Much has been written on the ac and dc Josephson effects and its numerous applications. The intention in this section is not to quantitatively derive relevant equations from first principles, but to qualitatively describe the characteristics of a Josephson junction required for an understanding of a SQUID.

A Josephson junction is merely a superconducting "weak link" such that a phase difference of the macroscopic wavefunction may exist across the link. If the junction is part of a superconducting ring and a current, i, is induced in the ring in the presence of a magnetic field, the circulating current is a sinusoidal function of the phase difference, or

$$i = i_c \sin \Delta\theta.$$

where i_c = critical current of junction.

As developed above, $\Delta\theta$ depends on the magnetic flux threading each side of the junction and this is of prime concern in the RF SQUID.

If the current through the junction (and hence its phase difference) is varying with time, a dc voltage, V, appears across the junction, such that

$$\frac{2eV}{h} = \dot{\Delta\theta}.$$

This can be considered a quantum of energy transfer (free of dissipation) across the junction, where the energy quantum $h\nu = 2eV$.

We can also equate an additional current term due to this induced voltage and the resistance of the junction, R, to V/R. Of course, $V = L\dot{\phi}$, where L is the inductance of the ring and ϕ is the change in flux threading the ring. In practice,

$$\frac{L\dot{\phi}}{R} \ll i,$$

thus this current term is usually not important. Rather, the junction acts as a lossless shorted turn in the ring except when $\Delta\theta = n\pi$, at which point a transition occurs, i.e., the junction is non-conducting and the ring changes its quantum state. Only then is an additional flux quantum allowed to thread the ring.

c. The RF SQUID

Figure 5 illustrates the symmetrical single-point-contact RF SQUID. The entire structure is machined from niobium, and the point contact is a pointed niobium screw. This device has extreme temperature stability and is relatively insensitive to external fields. It is only sensitive to differential fields, which shift the trapped flux from one hole to another. In effect, this symmetrical two-hole SQUID functions as a ring with a single Josephson weak link.

Flux is coupled to the holes of the SQUID through two coils; an input coil couples external flux threading a sample to one side of the junction, while an RF coil is used to interrogate the quantum state of the ring.

The RF coil produces an ac shielding current in the ring, $i = i_c \sin\Delta\theta$, so that the flux threading the ring does not change. When, however, $\Delta\theta = n\pi$, the critical ring current is reached, the junction becomes non-superconducting, and the quantum state changes, allowing a fluxoid to enter (or exit). After transition, the junction again becomes superconducting and the ac shielding current again flows to quantize the flux in the ring. Transition, however,

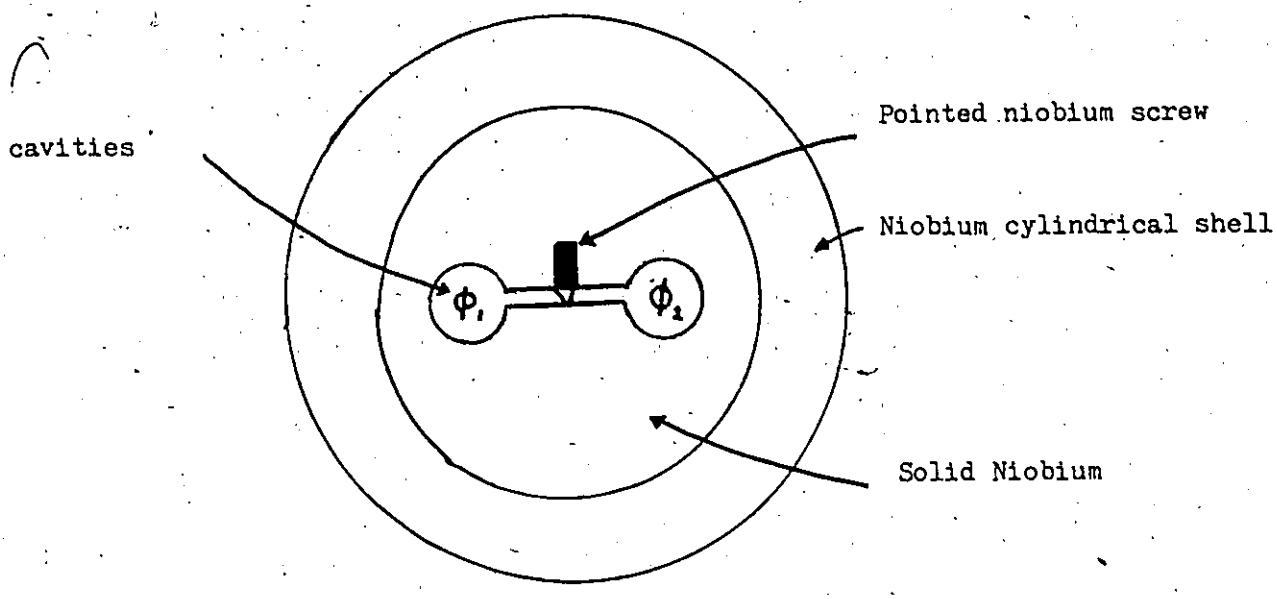

Fig. 5 Schematic diagram of a symmetrical single-point-contact RF SQUID.

temporarily reduces the level of oscillation in the RF coil, which then builds to its maximum. If no change occurs in the input coil, the transition recurs at the same level of oscillation and no change in the detected output is recorded. If, however, the input coil current is changed, a dc shielding current is superimposed on the ac component in the ring and the transition occurs at a different level of oscillation. The detected RF output therefore changes as a function of input flux threading the SQUID, as shown in Figure 6. The voltage driving the X-Y recorder, however, was the voltage drop in a feedback circuit from a phase sensitive detector (31). This technique permitted the time-independent transfer function to be recorded.

C. Application

a. Description of SQUID and electronics

A Superconducting Helium Electronics (SHE) Series 330 SQUID measurement system, including a Model 30 SQUID control unit and permanently adjusted TSQ sensor, were used in the SQUID experiments described later. Specifications regarding this apparatus is found in the System 330 Operating Manual.

In general, the following control selections and cabling configurations were used during operations:

SHE Model 30:

Output Jack: To X-Y recorder (Y input)

Detector output: To oscilloscope vertical input

Sync Jack: To oscilloscope external trigger

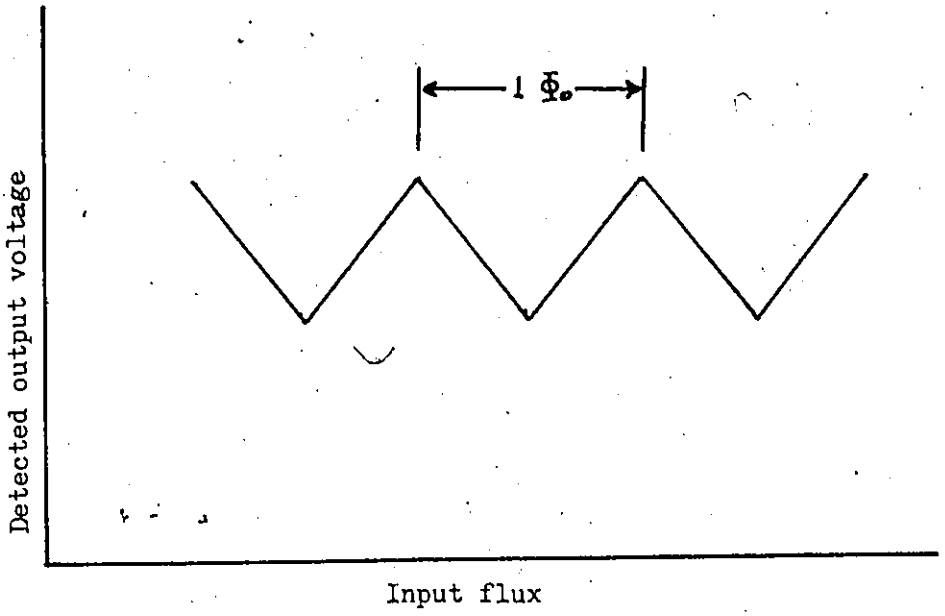

Fig. 6 Triangle SQUID transfer function showing detected voltage output as a function of flux in the SQUID (on the oscilloscope).

Note: The transfer function as displayed on the X-Y recorder appeared similar to the above, except that the output voltage from the electronic feedback circuit was time independent. The input flux change in the SQUID between consecutive peaks in this transfer function was estimated to be 2.8 Φ_o (see page 29).

INT FB selected

SENS: X100 selected

Notch Filter or 1 Hz selected

Function: Set 1 (transfer function on oscilloscope)

Slow to Fast (transfer function on X-Y recorder)

Model 504 Oscilloscope:

Vertical: 20mV/cm

Sweep time: 0.2 msec/cm

X-Y recorder:

X scale: .25 V/cm

Y scale: .5 V/cm

b. Sensitivity and noise

In practice, the sensitivity of a SQUID is usually limited by amplifier noise or external interference entering the dewar and coupled to the flux transformer. Some precautions used to shield against external interference are shown in Figure 7. The Johnson noise is generally negligible, since the circuit is resistive for only a short duration ($\sim \tau = L/R$) required for the quantum state to change. The fluctuating currents at this time have been estimated (27) and yield a limiting sensitivity of

$$\frac{\delta\Phi}{\Phi_o} \approx 2 \times 10^{-5}$$

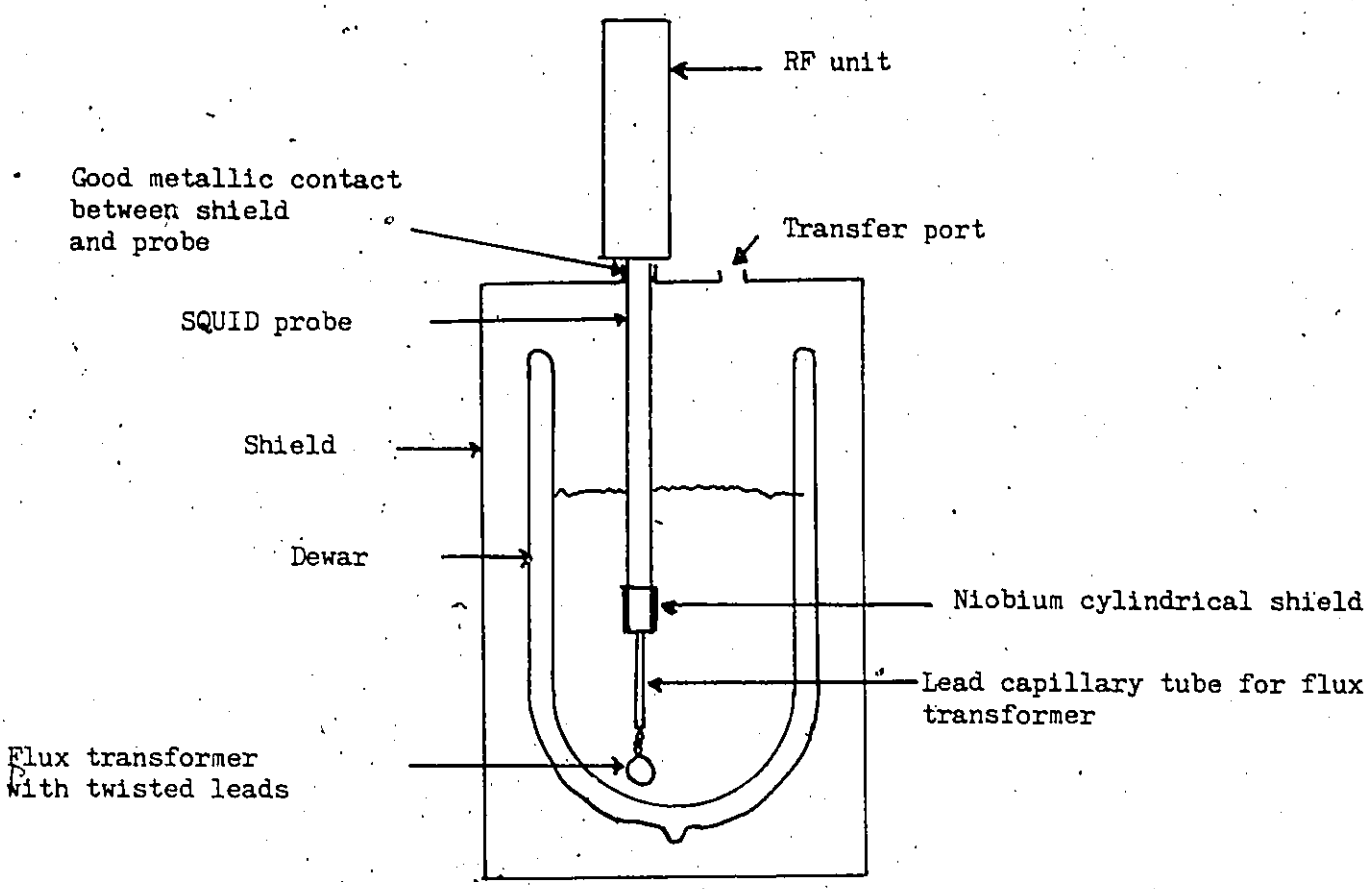

Fig. 7 Shielding of the SQUID and flux transformer against static discharge and RF interference.

c. The flux transformer

The magnetization measurements described later required that the magnetic flux to be measured be coupled to the SQUID through a flux transformer (see Figure 8). The transformer was comprised of 10 turns of 2 mil insulated niobium wire wound about the sample, as shown in Figure 11. The leads were twisted and threaded through a lead shield to two niobium screw terminals on the SQUID probe, terminating in the SQUID coil. The screw terminals were shielded with a niobium cylinder.

The sensitivity of the flux transformer, or the ratio of flux quanta sensed by the SQUID to the external flux sensed by the transformer coil, can be estimated by:

$$\frac{\Phi_{SQUID}}{\Phi_{ext}} = \frac{MN}{L_1 + L_2 + L_{leads}}$$

where M = Mutual inductance between SQUID coil and SQUID body

$\approx 2 \times 10^{-8}$H

N = number of turns of external transformer coil

= 10

L_1 = self inductance of transformer coil

L_2 = self inductance of SQUID coil

$\approx 2 \times 10^{-6}$H

L_{leads} = Lead inductance

$\approx 3 \times 10^{-7}$H/m x .15m = 5×10^{-8}H

L_1 may be estimated by

$$L_1 = \frac{a^2N^2}{9a + 10b} \mu H$$

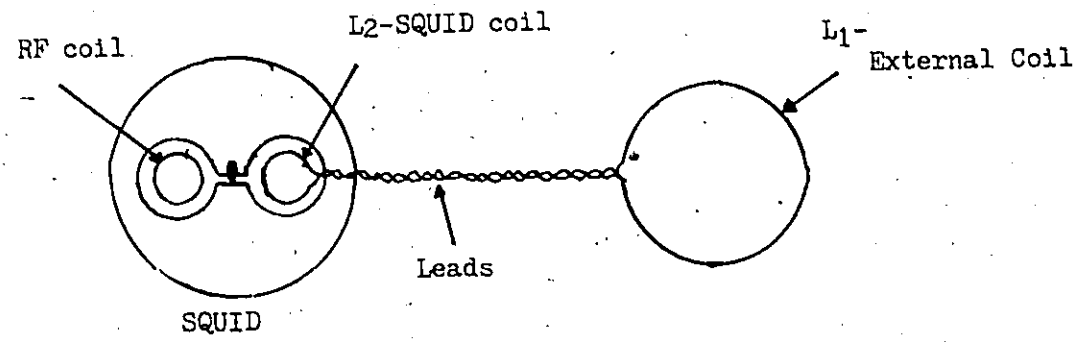

Fig. 8 SQUID flux transformer

where a = transformer coil radius in inches

$\approx .0093$

b = transformer coil length in inches

$\approx .0295$

Thus, $L_1 \approx 2.3 \times 10^{-8}$H.

Therefore, $\frac{\Phi_{SQUID}}{\Phi_{ext}} \approx .1$,

or every 10 fluxoids sensed by the external transformer coil yields a change of one Φ_o within the SQUID.

d. Calibration of feedback output voltage

As previously mentioned, the voltage driving the X-Y recorder was the voltage drop in a feedback circuit from a phase sensitive detector. As flux changes are sensed by the SQUID coil, a phase change is detected between the audio oscillator reference and the RF oscillator. This phase change is measured as a linear voltage response from the output of the phase sensitive detector, generating the "rising" slope of the transfer function on the X-Y recorder. The voltage would increase indefinitely if it were not for an electronic reset at the maximum of 5 volts, causing the "declining" slope of the transfer function. It was experimentally found (32) that, with the above SQUID settings, an output voltage of 1.8 volts/Φ_o could be expected. Therefore, each cycle of the transfer function corresponded to 5 v/cycle $\div$ 1.8 v/Φ_o = 2.8 Φ_o/cycle.

III. EXPERIMENTAL ARRANGEMENT AND PRODEDURES

A. Introduction

The object of the experiments described in the following sections was to detect small (i.e., at the quantum level) changes in the axial magnetic flux as a transport current was varied in a cylindrical sample in an axial magnetic field. Although a change in the transport current produces a change in the purely azimuthal field, the resultant field at the surface of the cylinder is helical, since $H_{total} = (H_z^2 + H_\theta^2)^{\frac{1}{2}}$. A change in the transport current would therefore presumably cause fluxons to enter (or exit) the surface, each of which has an axial component, and produce a measurable change in the axial magnetization in discreet steps as fluxons enter (or exit) the sample. The theoretical behaviour of the bulk magnetization is complicated by the spiralling movement of the fluxons into the bulk, which causes a gradient in direction as well as magnitude of the internal magnetic field. These experiments were not designed to shed additional light on this complicated magnetic behaviour, but were intended only to detect quantum changes in the axial flux and to perhaps determine the sense of the magnetic moment. The experiments were also intended to examine the feasibility of using a Superconducting Quantum Interference Device (SQUID) coupled to a flux transformer in measuring small changes in axial magnetization of samples.

Two experimental arrangements were used in performing the experiments. In the first arrangement, herein called the "classical" approach, a pick-up coil surrounded the sample to detect sample magnetization. Although

this arrangement suffered from extreme magnetic shielding problems, the arrangement will be described in some detail to present the unique approach used in balancing the series-connected, oppositely wound coils, as well as describe the method of winding a bifilar heater on a very fine (2 mil diameter) sample of Niobium.

The second arrangement, herein called the "SQUID" approach, used an improved magnetic shielding technique and a flux transformer surrounding the sample coupled to a SQUID to detect small changes in the axial flux threading the sample. The experimental results discussed later mainly refer to results obtained from using this arrangement.

B. Classical approach

a. Physical arrangement

The physical arrangement for the Classical approach is shown in Figure 9. A sample of 2 mil diameter Niobium wire was mounted between two pairs of copper blocks, through which the transport current was applied. The sample ends were wrapped in Indium foil and firmly clamped between each pair of copper blocks to minimize contact resistance. Parellel wires (one on each side of the pick-up coil) were used to supply the transport current to minimize the detection of the magnetic field surrounding these wires by the coil. Another set of copper blocks clamped to the sample provided leads to measure the voltage across the sample during flux-flow or normal conditions. A non-inductively wound heater coil surrounding the sample provided

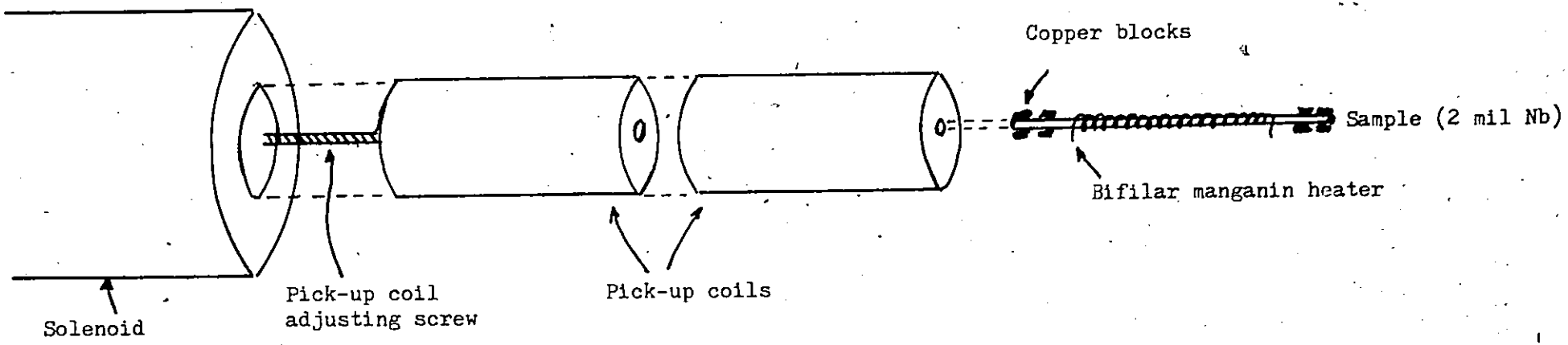

Fig. 9 Classical approach-physical arrangement

the heat required to bring the sample to the normal state and therefore erase its superconducting magnetic history.

The sample assembly (described in more detail below) was mounted on the axis of a pick-up coil (160,000 turns of #46 Copper). An identical coil, oppositely wound, was connected in series with the first coil to minimize the effect that an axial field change has on the induced voltage of the coil pair. In effect, any change in axial magnetization of the sample would induce a voltage across the first pick-up coil ($V = N\frac{d\phi}{dt}$) proportional to the rate of change of flux. However, any change to an applied axial field would induce equal and opposite voltages in the coil pair (assuming the coils were sensitively balanced) and therefore make the coil pair relatively immune to applied or extraneous magnetic field changes.

A copper solenoid surrounded the sample-pick-up coil arrangement to provide an axial magnetic field of 0 to 300 Gauss. The entire apparatus was then immersed in a bath of liquid helium (i.e., 4.2°K) and the outside dewar was wrapped in several sheets of "μ-metal" to minimize the effect of extraneous magnetic fields.

i) Details of the sample assembly

It was found that winding a bifilar heater of #38 manganim wire around 2 mil Niobium was extremely difficult due to the brittleness of Niobium. The procedure finally adopted is therefore described in detail.

A twenty centimetre length of #18 enamelled copper wire was inserted in a hollow pyrex tube, slightly stretched and firmly mounted on a coil winder. A bifilar heater wire was then wrapped about the #18 wire, to a

length slightly more than the length of one pick-up coil. Unwaxed dental floss was placed along the length of the heater, in contact with it, and a coat of epoxy cement was applied to the heater and floss. When the cement was dry, the pyrex tube was slid over the heater and both ends of the tube were cemented with epoxy to the heater. When dry, the assembly was removed from the coil winder and the #18 wire was stretched to reduce its diameter, permitting it to be removed from the centre of the heater coil. The sample was then threaded through the core of the heater and permitted to remain in contact with one side of the core. With a hypodermic needle, dilute white glue was inserted through the core to surround the sample. When this was dry, the sample was cemented with epoxy to both ends of the glass tube. The entire assembly was then mounted on the axis of one pick-up coil, as shown in Figure 9.

i) Details of balancing the pick-up coils.

The two pick-up coils had to be balanced to achieve a null voltage response to changes in the external field. This was accomplished first at room temperature by inserting the coils within the solenoid and varying the applied axial magnetic field and by removing turns from one coil until a balance was achieved. A similar procedure was followed at liquid helium temperature, since thermal compression changed the balance slightly. It was found, however, that the delicate balance could not be maintained, i.e., a balanced coil pair would become unbalanced during an experimental run or between consecutive runs. An arrangement was therefore developed to vary the balance while the assembly was immersed in liquid helium. The entire

assembly (pick-up coils with sample) was made to slide within the core of the solenoid from an adjusting screw located outside the dewar. This technique used the slight inhomogeneity of the solenoid's field to achieve a precise balance.

b. Electrical arrangement

The electrical arrangement for the Classical approach is shown in Figure 10. The circuit provided for a .5Ω shunt across the sample to prevent the sample from burning when the critical current was reached. It also provided for a bias transport current through the sample of approximately .46A and a variability range for the transport current of about 700 μA. The current could be adjusted in 1μA steps throughout this range.

The output voltage from the pick-up coils was converted to a signal proportional to the sample magnetization by a Princeton Applied Research Model 215 electronic integrator. The integrator output drove the Y-axis of an X-Y recorder while the X axis was driven from either the voltage drop across a shunt in the solenoid circuit (signal was proportional to applied axial field) or the voltage drop across a shunt in the circuit delivering current through the sample (signal was proportional to bias current).

The voltage monitor across the sample was a Keithley Model 150B μV-ammeter. Any deflection on this meter indicated either a flux-flow or normal condition of the sample.

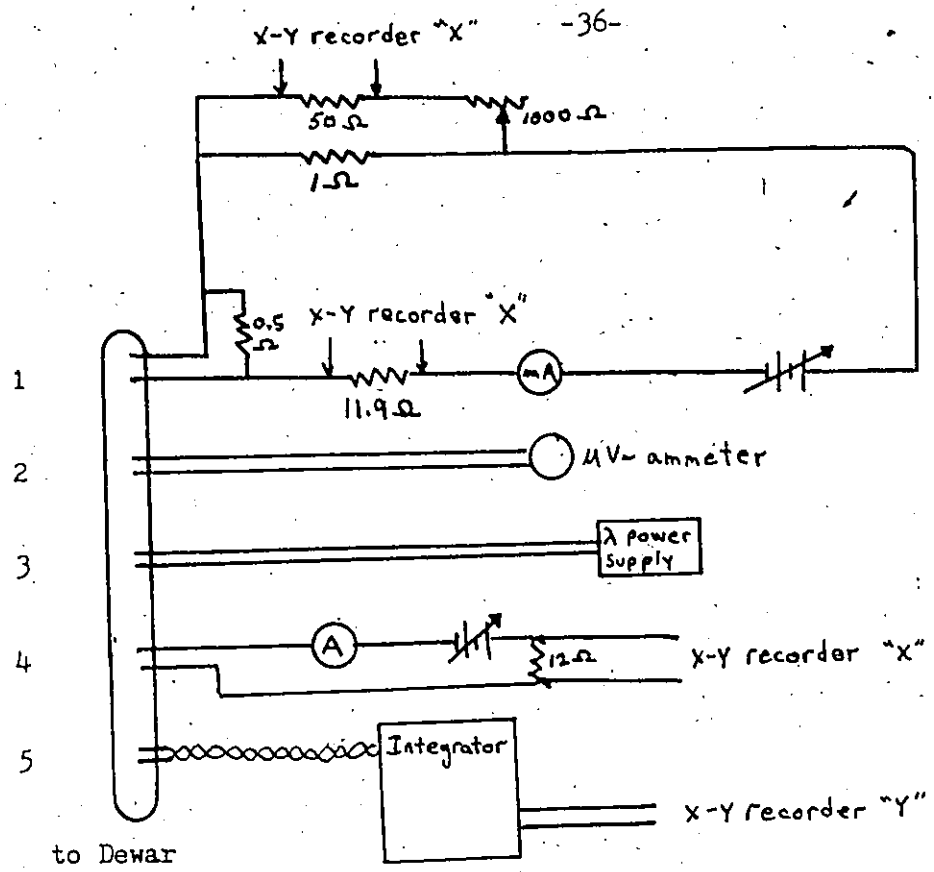

Lead Legend:

1 - To sample ends to provide transport current

2 - To tap on sample to determine onset of flux-flow

3 - To sample heater of bifilar manganin

4 - To solenoid

5 - To pick-up coils

Fig. 10 - Classical approach-external electrical arrangement

c. Experimental procedure

Prior to all experimental runs, the pick-up coils were adjusted in liquid helium by passing a transport current through the sample greater than the critical current to prevent sample magnetization and by slowly changing the applied axial magnetic field, H_a, generated by the solenoid. The external adjusting screw for the pick-up coils was turned until a null integrated voltage response from the coils was observed for the entire range of H_a.

An attempt was made to produce magnetization curves for a variety of sample magnetic histories. First, the sample was cooled in only the earth's magnetic field. An axial magnetic field of either 0, 100, or 300 Gauss was applied, all three field strengths being examined in succession. Next, a magnetization run, $\langle M_z \rangle$ versus bias current, I_b, was attempted as I_b was cycled from 0 to .46 A. Finally with $\langle I_b \rangle$ at either 0 or .46 A, I_b was varied over a range of a few hundred μA (ΔI) and average sample axial magnetization observed as a function of ΔI.

Second, the sample was cooled in the earth's magnetic field, and a transport current of 0 or .46 A was applied, both currents being examined. Next, a magnetization run, $\langle M_z \rangle$ versus H_a, was attempted as H_a was cycled from 0 to 300 Gauss. Finally, with H_a at either 0, 100, or 300 Gauss, I_b was varied over a range of a few hundred μA (ΔI) and average sample axial magnetization observed as a function of ΔI.

The third and fourth procedures were similar to the first and second, except that an axial magnetic field of 100 or 300 Gauss was applied in the normal state, prior to cooling past the superconducting transition temperature, T_c. Heating above T_c was accomplished by passing a .5 A current through the bifilar manganin heater wound about the sample. When

a transport current was applied to the sample, the voltage monitor across the sample abruptly changed from 0 to .2 volts at transition to the normal regime.

Finally, an attempt was made to determine the critical transport current, I_c, for a variety of magnetic histories of the sample and for a variety of applied axial magnetic fields. Again, the voltage monitor across the sample abruptly changed when I_c was reached.

C. SQUID approach

a. Physical arrangement

The physical arrangement for the SQUID approach is shown in Figure 11. A sample of 3 mil niobium-tantalum wire was mounted between two pairs of indium coated copper blocks, through which a transport current was applied. Another set of copper blocks clamped to the sample provided leads to measure the voltage across the sample during flux-flow or normal conditions. A non-inductive (bifilar) heater coil of #38 manganin wire was wound directly about the sample to provide the heat required to bring the sample to the normal state.

A flux transformer consisting of ten turns of 3 mil insulated niobium wire was wound on the heater, and the twisted transformer ends were encased in a lead sheath and connected by niobium screw contacts to the SQUID.

To provide a known magnetic calibration field, a calibration coil consisting of 4 turns of #34 copper wire was wound around the flux trans-

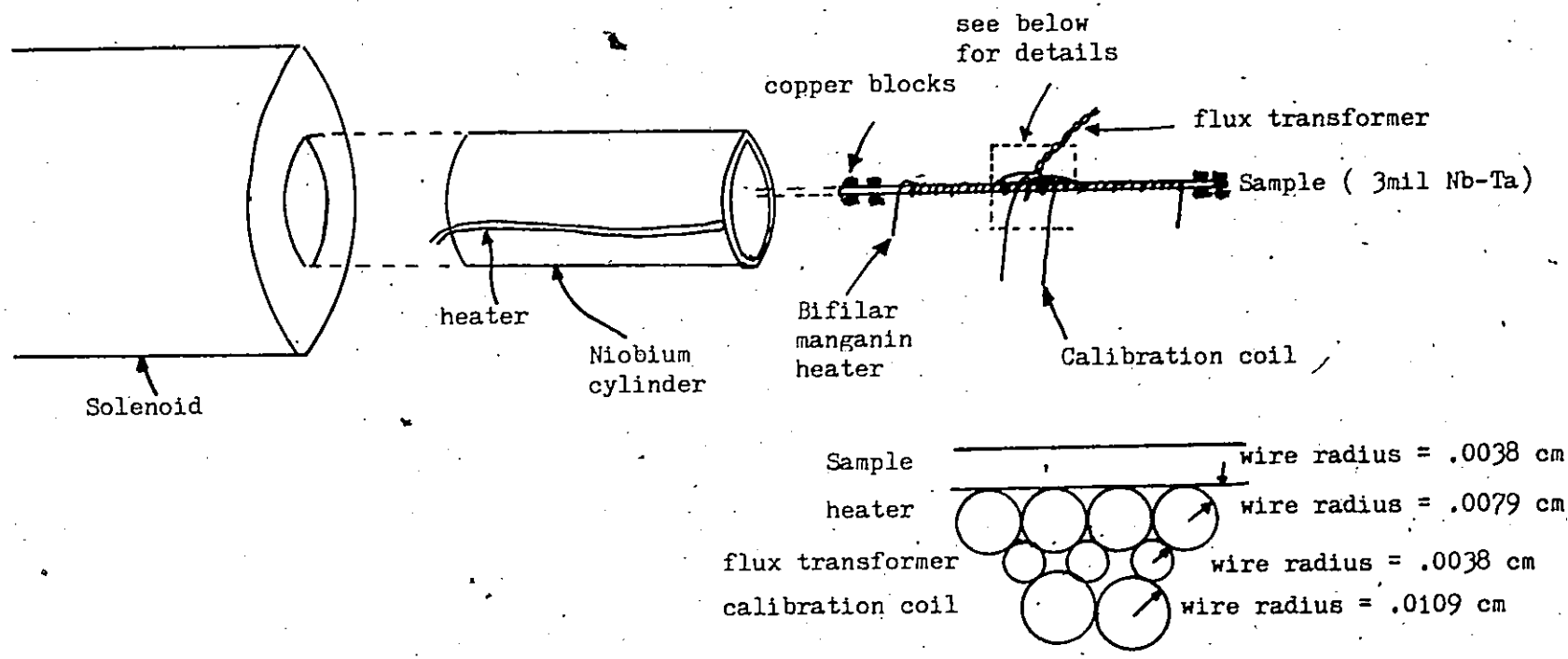

Radius flux transformer = .0235 cm

Radius calibration coil = .0382 cm

Fig. 11 SQUID approach-physical arrangement

former-heater-sample assembly. The assembly was then rigidly mounted with epoxy cement in a pyrex tube.

The sample assembly was inserted on the axis of a niobium cylinder, which served to trap any applied axial magnetic field and to effectively shield (29, 30) against extraneous fields. A manganin heater wire was mounted in thermal contact on one side of the cylinder to permit trapping of a known applied field by breaking the lossless current in the cylinder with the application of heat above its transition temperature.

The niobium cylinder-sample arrangement was then mounted on the axis of a superconducting solenoid capable of producing an axial magnetic induction of 0.645 Gauss per applied mA. The solenoid was enclosed in a lead-plated copper cylinder to provide additional magnetic shielding and firmly mounted to a support suspended from the laboratory ceiling. The SQUID probe was encased in a niobium cylinder shield and mounted to the same support.

A metallic dewar, grounded to the SQUID probe, was used to provide shielding against static discharge. The dewar itself was raised or lowered on a manual crane to provide access to the experimental apparatus.

b. Electrical arrangement

The electrical arrangement for the SQUID approach is shown in Figure 12. Adjustable current sources provide the current for the sample heater to drive the sample normal (~60mA), for the niobium cylinder heater (~400mA), and

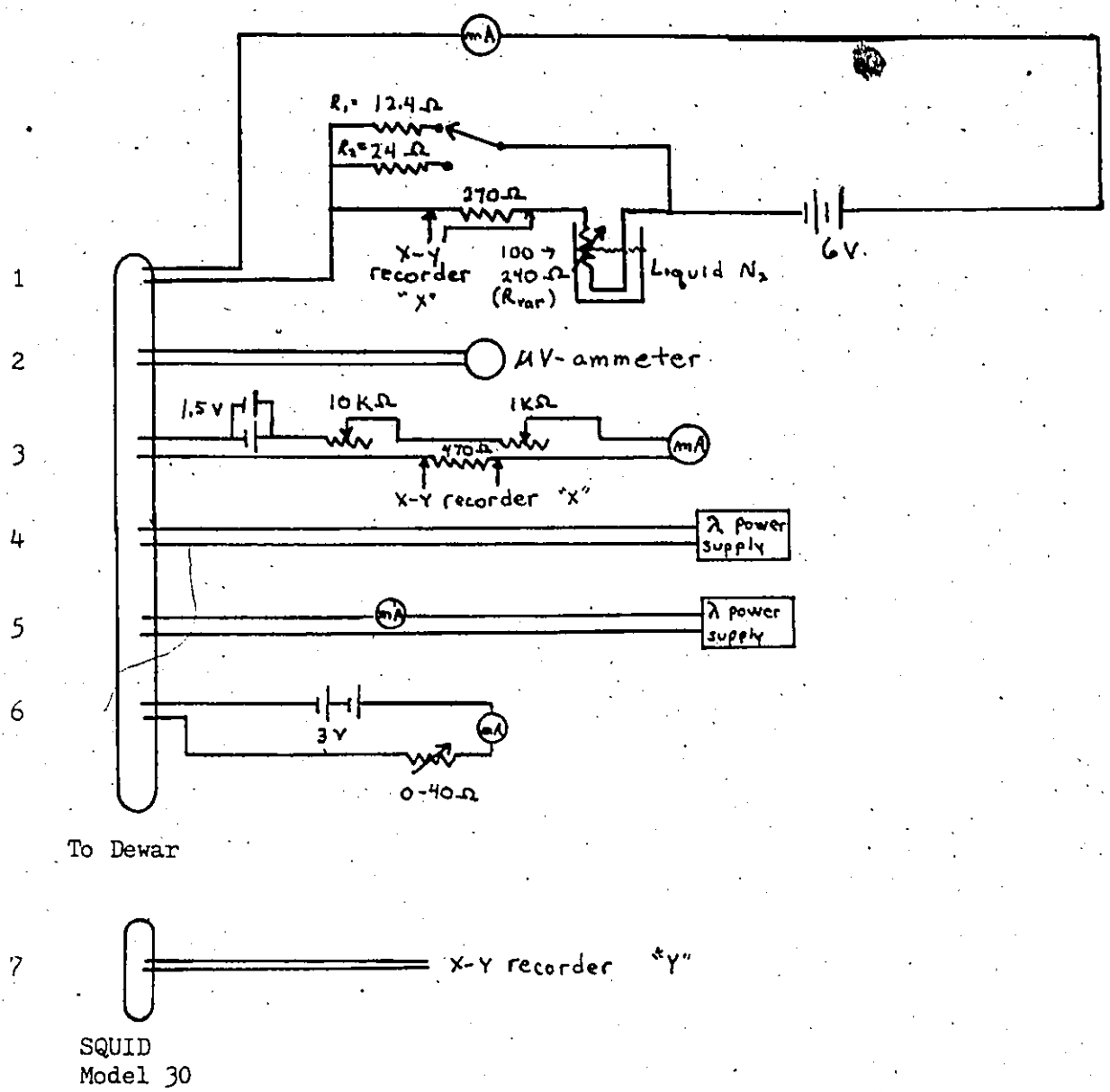

Lead Legend:

1 - To sample ends to provide transport current

2 - To tap on sample to determine onset of flux-flow

3 - To calibration coil

4 - To niobium cylinder heater

5 - To superconducting solenoid

6 - To sample heater of bifilar manganin

7 - Detected output from SQUID feedback circuit

Fig. 12 SQUID approach-external electrical arrangement

for the superconducting solenoid to provide an axial magnetic field.

The circuit which provided transport current through the sample enabled bias currents of either .26 A or .50 A to be selected by switching between R_1 and R_2. A variable resistance, R_{var}, in parallel with R_1 or R_2, was made from several hundred turns of #34 copper wire wound about a 4 cm bakelite tube which was slowly lowered into a dewar of liquid nitrogen. This technique provided a resistance variability of 240 to 100 ohms, or a transport current change of a few μA to 5 mA. Most importantly, the current change was extremely smooth, with no perceptible fluctuations as would be the case with a helipot.

A shunt in the transport current circuit provided a voltage drop proportional to the change in current, ΔI, through the sample. This voltage drove the X-axis of an X-Y recorder while the Y-axis was driven from the output of the SQUID electronics. Additional information on the SQUID electrical circuit is found in Section II of this thesis.

The voltage monitor across the sample was a Keithley Model 150B μV-ammeter. Any deflection in this meter indicated either a flux-flow or normal condition of the sample.

c. Experimental procedure

The SQUID was carefully calibrated so that a change of flux of one Φ_o through the SQUID coil resulted in a single cycle of the triangle waveform on an oscilloscope.

Next, the efficiency of the flux transformer was determined. A measured current was slowly applied to the calibration coil, thus causing a known (approximately) axial magnetic field to be incremented within the flux transformer. A signal proportional to the current drove the X-axis of an X-Y recorder, while the SQUID output drove the Y axis. Thus, a known change in external axial flux caused a change of a single Φ_0 within the SQUID at each cycle of the triangular waveform on the oscilloscope.

Finally, the change in the axial magnetization of the sample in three magnetic regimes was determined as the bias transport current was slowly changed. First, for the diamagnetic regime, the sample was cooled in the presence of only the earth's field and then an axial magnetic field was applied. Second, for the paramagnetic regime, the sample was cooled in the presence of a higher axial field which was then reduced. Third, for the non-magnetic regime, the sample was cooled in the presence of an applied axial field which was held constant. In all cases, the final applied field was, successively, 0, 50, 100, and 300 Gauss. As described earlier, the superconducting solenoid contained the niobium tube which surrounded the sample. For changes in the applied field induced by the solenoid to be perceived by the sample, the niobium tube heater was used to break the continuity of the lossless currents in the cylinder and permit the trapped flux to escape.

At each increment of trapped magnetic field, bias transport currents of $\pm$.26 A and $\pm$.50 A were passed through the sample. The transport current was then slowly changed by gradually immersing the variable resistor in liquid nitrogen. The change of current was monitored on the X-axis of an X-Y recorder and the SQUID output drove the Y-axis. Thus, by comparing this recording with that of the calibration run, it was possible (in principle) to determine the change in axial magnetization (of the order

of a few flux quanta) with change in the bias transport current. The bias current was applied in both the positive and negative senses to minimize the effects of sample geometry on the results.

The critical current, I_c, of the sample was also determined for a variety of magnetic conditions. The transport current was slowly incremented while the voltage across the sample as well as the triangular waveform on the oscilloscope were monitored.

IV. EXPERIMENTAL RESULTS, INTEPRETATION, AND ANALYSIS

A. Classical approach

a. Magnetization measurements

Extreme difficulties were encountered in performing magnetization runs using the Classical approach. Although a balance of the two pick-up coils could be accomplished with the external adjusting screw (as described in section III), the coils were extremely sensitive to extraneous magnetic field gradients in spite of the various precautions taken to provide magnetic shielding. For example, any movement within several meters of the dewar produced a noticeable deflection of the integrated pick-up coil output. Also, a current to the solenoid produced eddy currents within the solenoid's copper end plates sufficient to mask the magnetization effects of the sample. These could be reduced, but not entirely eliminated, by incrementing the current to the solenoid at an extremely slow rate. Therefore, no useful magnetization measurements were made.

These problems, of course, could have been reduced through additional shielding techniques and solenoid design. However, since the main goal of the Classical approach was to provide preliminary magnetization curves prior to a more detailed analysis of the curves using a SQUID, it was decided that the experimental effort could best be concentrated on the SQUID approach.

b. Critical current measurements

Similar obstacles were encountered in passing a transport current

through the niobium sample. This very fine (2 mil) sample was chosen to provide a relatively high change in magnetic field at its surface due to a small change in its transport current. However, this sample proved to be very delicate and often broke from thermal contraction when cooled to liquid helium temperature. For the samples that remained intact, the critical current varied considerably. The best estimate of I_c for this sample was 0.29 A, which yielded a J_c of 14,300 A/cm^2. A change of I_c with applied axial field could not be detected within the experimental error of this arrangement.

B. SQUID approach

a. Interpretation of the SQUID transfer function

One of the goals of the SQUID approach was to measure a single fluxoid entering or exiting the sample as a transport current was varied. Since the efficiency of the flux transformer was computed to be about 0.1 (see Section II), a 10 Φ_o change at the sample would be a single Φ_o change at the SQUID. Since 2.8 Φ_o corresponded to a single cycle of the X-Y transfer function (Figure6), each cycle represented a change of 28 fluxoids threading the sample. Would each Φ_o at the sample, however, be evident from steps in each cycle of the transfer function? Although it should be theoretically possible to see a stepped transfer function and therefore individual flux quanta changes threading the sample, none could be seen on the rising slope of the triangles measured on the X-Y recorder. This is probably due to the small signal of individual Φ_o's being imbedded in the inherent noise of the experiment, thus preventing greater amplification from improving the resolu-

tion. Occasionally, steps could be seen on the decreasing slope of the triangles, but these can only be interpreted as thermal fluctuations in the SQUID electronic reset circuit.

b. Calibration runs

Several calibration runs were performed to experimentally verify the efficiency of the flux transformer. A known current increment, ΔI, was passed through the calibration coil, producing an axial magnetic field of $B_z = \mu_o N \Delta I$. In the experimental arrangement reported here, N = 4 turns / 7.5×10^{-4}m = 5.33×10^3 turns/m. The change in current required for one cycle of the SQUID transfer function was 70 μA. Therefore, $\Delta B_z = 4.7 \times 10^{-7}$ Wb/m^2 = 4.7×10^{-3} Gauss. Since the cross-sectional area of the flux transformer is 1.7×10^{-3}cm^2, we would expect a flux change corresponding to ΔB_z of $\Delta\phi = \Delta B_z A = 39 \Phi_o$. This result was experimentally reproducible to within 1 Φ_o.

The above calculation, however, assumed that the calibration coil was infinitely long and therefore that end effects could be ignored. The actual configuration was a calibration coil of nearly the same length as the flux transformer, which would result in a lower detected field than that calculated. The calculation also assumed that the flux transformer was on the axis of the calibration coil rather than considerably off-axis, as was the case. Again, the field sensed by the flux transformer would be less than that calculated. Since the calibration run thus predicted that each triangle of the SQUID transfer function on the X-Y recorder corresponded to somewhat less than 39 Φ_o and the SQUID calculation (above) yielded a value of 28 Φ_o per triangular cycle, the latter may be considered the best estimate for the efficiency of the flux transformer / SQUID / electronics.

c. Magnetization measurements

Figure 13 shows a typical SQUID transfer function in performing a magnetization run. To convert this into the more familiar magnetization curve ($\Delta\langle M_z\rangle$ versus ΔI), ΔI corresponds to the average current between peaks of the triangular transfer function and $\Delta\langle M_z\rangle$ is directly proportional to $2\Phi_0$. Thus, each run performed with a fixed axial magnetic field and fixed bias current yields a slope of the magnetization curve. However, the coordinate location of that slope on the magnetization curve is not known, since the SQUID was only equipped to show increments ($\Delta I/\Phi_0$), or slope. Therefore, the sense of magnetization (diamagnetic or paramagnetic) could not be determined from this arrangement.

Most magnetization runs, performed at various bias currents and applied axial fields, were very similar to Figure 13; that is, the $\Delta I/\Phi_0$ varied only by several percent to a maximum of 24% - much less than expected if only axial magnetization were being recorded. The most probable explanation is that most of the flux sensed by the transformer is not axial flux but rather azimuthal flux due to the loop in the transformer leads prior to its enclosure in the lead capillary tube. A simple calculation verifies the reasonableness of this explanation. The change in azimuthal field, ΔB_ϕ, due to a change in current in a wire is

$$\Delta B_\phi = \frac{\mu_0 \Delta i}{2\pi R} .$$

With R the radius of the flux transformer and Δi = 1.84mA (from Figure 13), ΔB_ϕ = .0157 Gauss.

If the area of the loop in the transformer leads is only 1/3 the cross-sectional area of the flux transformer coil, this ΔB_ϕ A corresponds

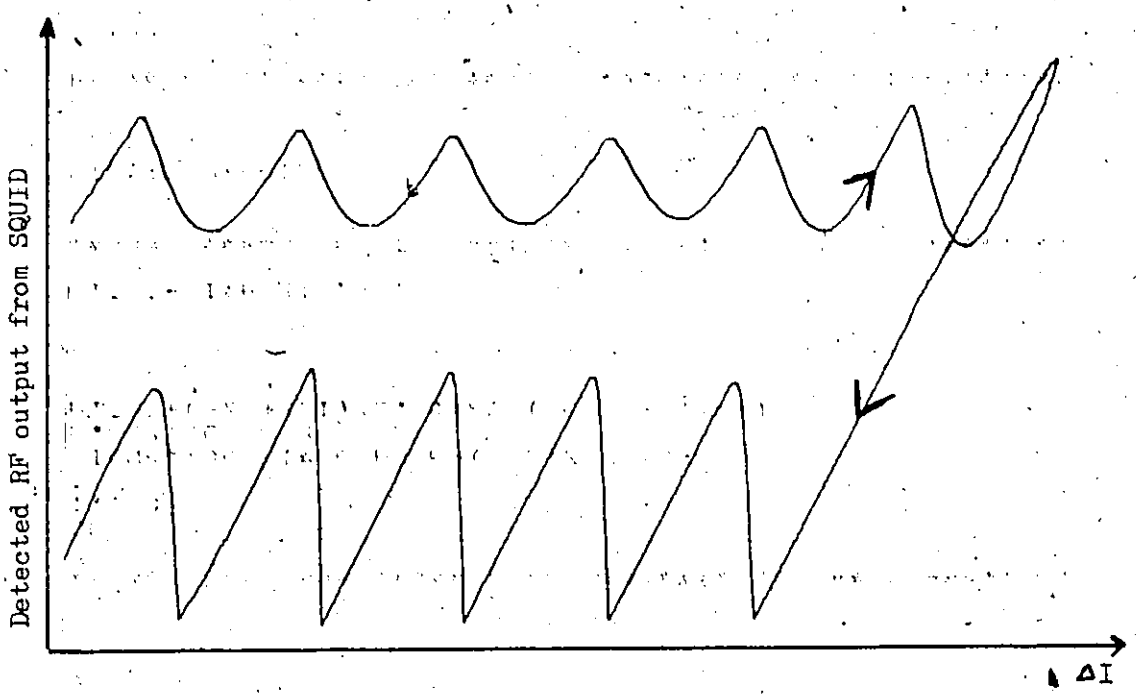

Bias current, I_b = + 0.26A

Applied field, B_a = Earth

ΔI (peak-to-peak) ≈ 1.84 mA

Fig. 13 Typical SQUID transfer function during experimental run

to $28\Phi_0$, or the calibrated peak-to-peak flux change in the transfer function. Such an estimate for the area of the loop is entirely reasonable, thus ΔB_ϕ seems to be the dominant mechanism coupling flux to the SQUID.

Some interesting trends in axial magnetization of the sample may be explored, however, since the effects of axial magnetization and induced azimuthal fields are superimposed.

General trends in axial magnetization:

i) No perceptible change in response of the SQUID was noted to small changes in sample current as a positive or negative bias current was imposed. This indicated a very symmetrical geometry of the sample and flux transformer.

ii) If the transport current was slowly cycled by alternately increasing and decreasing the current through the sample, the value of $\Delta I/\Phi_0$ was reduced when <u>decreasing</u> the current, relative to its value when the current was increasing. This was only evident during the first cycle after cooling with no noticeable change in subsequent cycles. This was apparently a consequence of irreversible magnetic behaviour during the first cycle.

iii) There was an increase in the value of $\Delta I/\Phi_0$ with increased applied axial field and with increased bias current. This would be as expected, since the increased total magnetic field, proportional to both applied axial field and the in-

duced azimuthal field, causes an increase in the pinning force. Hence, a greater current change is required to overcome pinning and cause fluxons to enter or exit the sample.

iv) In the absence of a bias current, the value of $\Delta I/\Phi_o$ was found not to vary with the applied axial field. This may be interpreted as the small current change being unable to generate a sufficient field to penetrate the surface barrier of the sample and cause a change in axial magnetization. The $\Delta I/\Phi_o$ was probably due entirely to the induced azimuthal field.

v) An interesting regime was accidently noted and several experimental runs attempted to explore that regime. When the sample was cooled while carrying a bias transport current (as opposed to previous runs in which the sample was cooled prior to a transport current being imposed), it was found that a flux-flow resistive state existed. That is, a voltage drop across the sample was noted, and the SQUID transfer function indicated a sample magnetic response slightly different from that of the purely superconducting regime. For example, there was an increase in $\Delta I/\Phi_o$ as compared to the superconducting state, which varied from +2% of the superconducting state at no applied axial field to +24% of the superconducting state at 300 Gauss applied field. Also, the sample exhibited completely reversible behaviour, showing no change in $\Delta I/\Phi_o$ with

increasing or decreasing current. This was consistent with the behaviour of the surface sheath, explored in Section I. Finally, the value of $\Delta I/\Phi_o$ was found to increase with a greater applied axial field, consistent with the increased pinning noted in the superconducting state.

d. Critical current measurements

Critical current measurements were made for several applied axial fields, but most results varied between runs and were not readily reproducible. The results obtained differed from previous published results (21), since the critical current apparently decreased for increased applied fields. The results obtained were

$$I_c \ (B_a = 0 \text{ Gauss}) = .65A$$

or $$J_c \ (B_a = 0 \text{ Gauss}) = 14{,}200 \ A/cm^2$$

$$I_c \ (B_a = 300 \text{ Gauss}) = .50 \ A$$

or $$J_c \ (B_a = 300 \text{ Gauss}) = 10{,}900 \ A/cm^2$$

C. Summary and Conclusions

Although the Classical approach was found to be not suited for measuring very small magnetization changes (without considerable shielding sophistication) and a single Φ_o was not detected using the SQUID, several results for this series of experiments were obtained. Considerable expertise was gained on the application of the SQUID to magnetization experiments using a flux transformer. In particular, the loop in the transformer leads was found to sense

the changes in azimuthal field and contribute substantially to the flux change in the SQUID. Trends in the experimental runs tended to verify known magnetic properties of Nb-Ta, but an unusual magnetic regime was also reported and investigated.

APPENDIX

REPRESENTATIVE SAMPLE OF SQUID TRANSFER FUNCTIONS

Note: X-Y Recorder Scale Factors

All runs: X = 0.25 V/cm
Y = 0.50 V/cm

Calibration: X = 15 mV/cm
Y = 0.50 V/cm

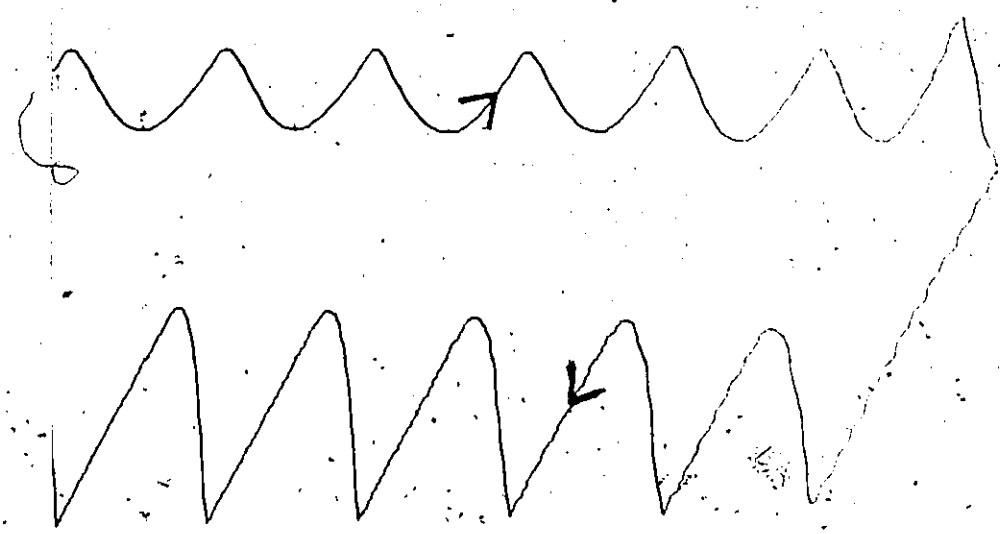

I_b = +0.26 A
B_a = Earth

Subsequent run (initial run on page 49)

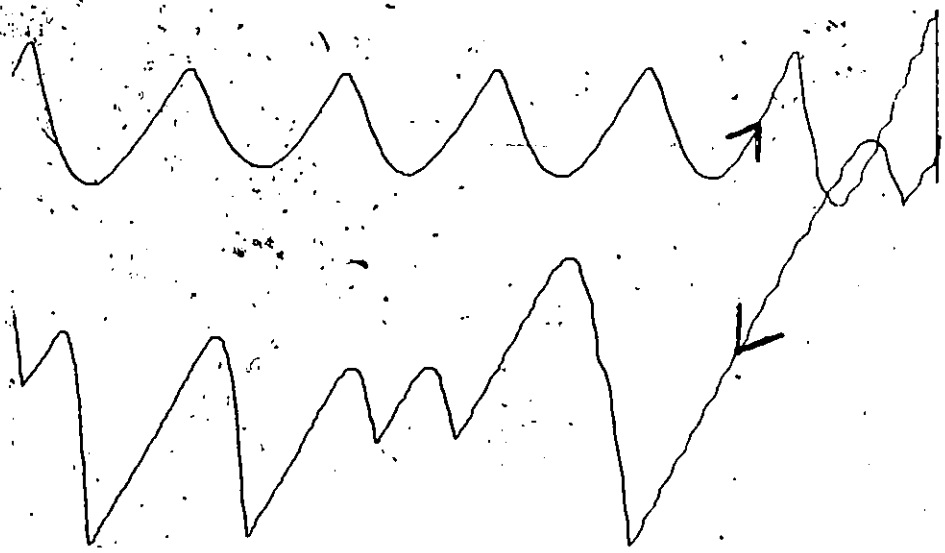

I_b = +0.26 A
B_a = Earth

Flux-flow voltage state

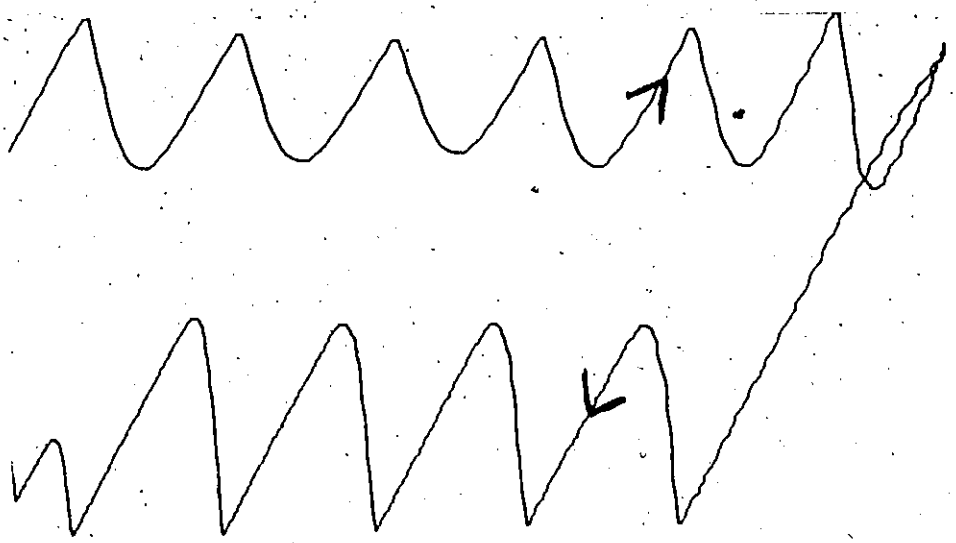

I_b = +0.26 A
B_a = 50 G

Initial run

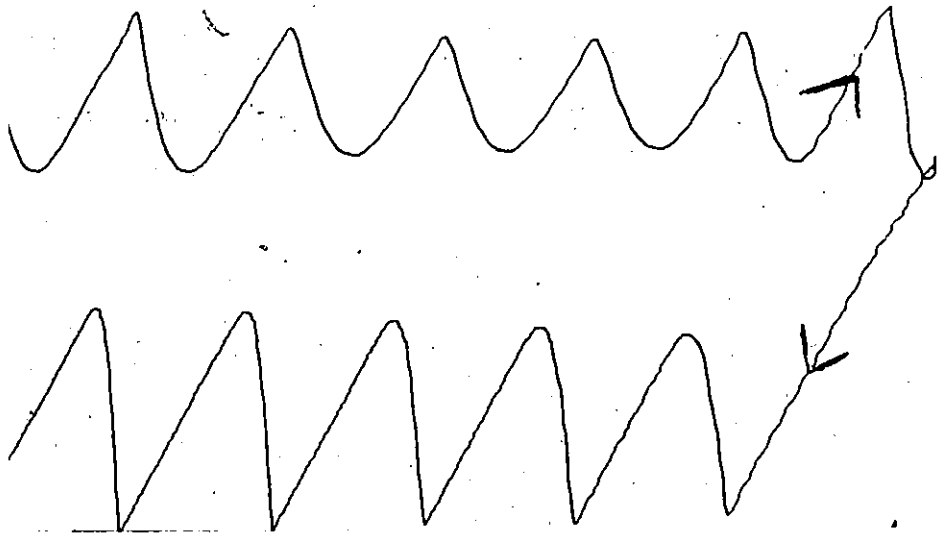

I_b = +0.26 A
B_a = 50 G

Subsequent run

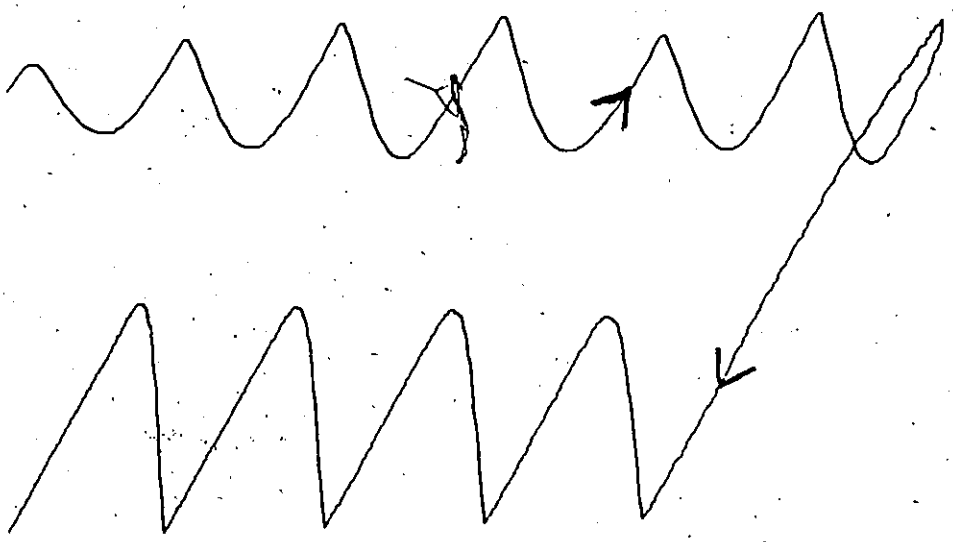

I_b = +0.26 A
B_a = 50 G

Flux-flow voltage state

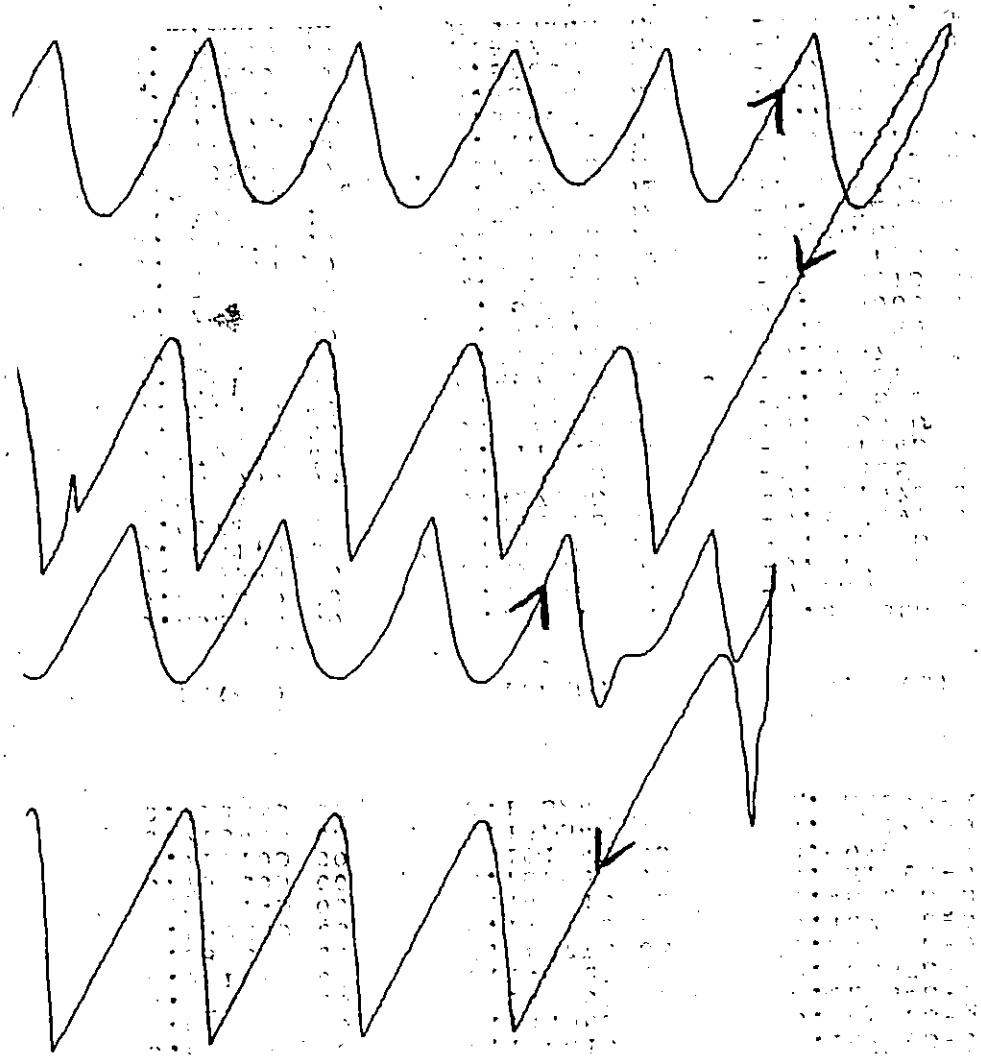

I_b = +0.26 A
B_a = 100 G

Initial run (bottom), subsequent run (top)

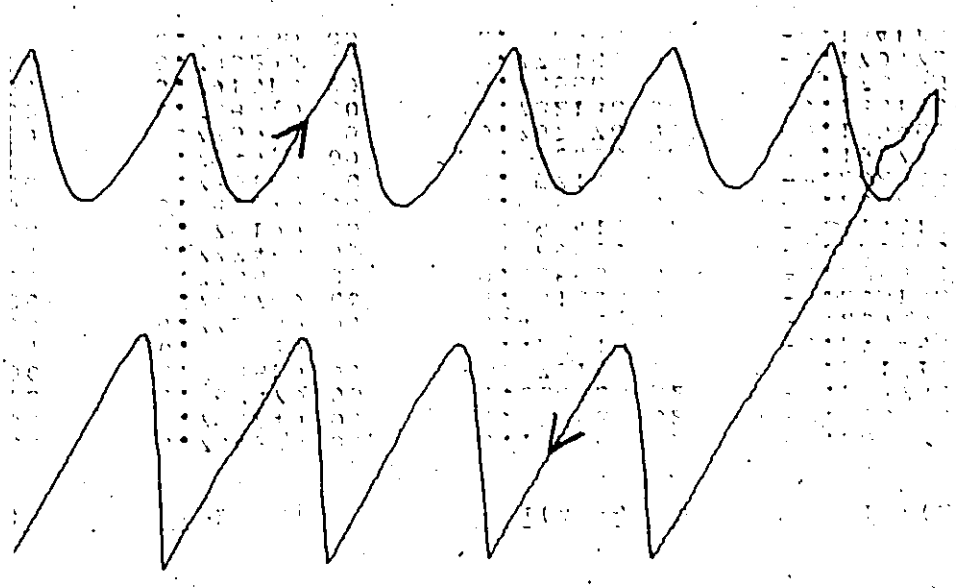

I_b = +0.26 A
B_a = 100 G

Flux-flow voltage state

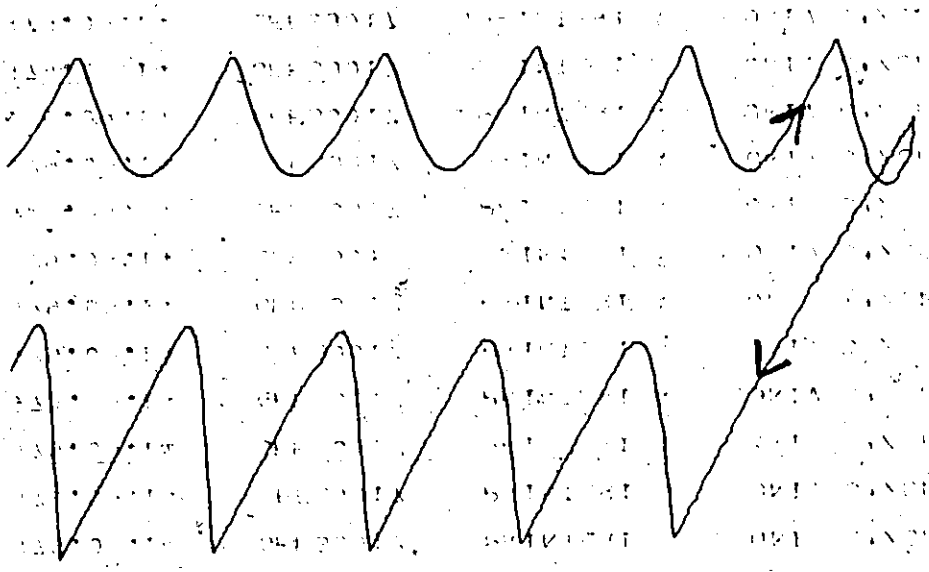

I_b = + 0.26 A
B_a = 300 G

Subsequent run

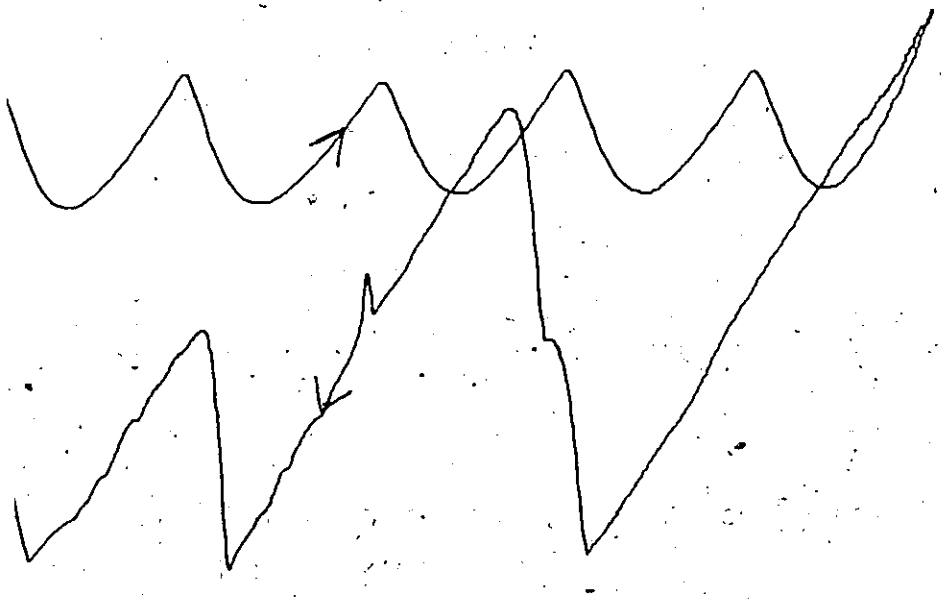

I_b = +0.26 A
B_a = 300 G

Flux-flow voltage state

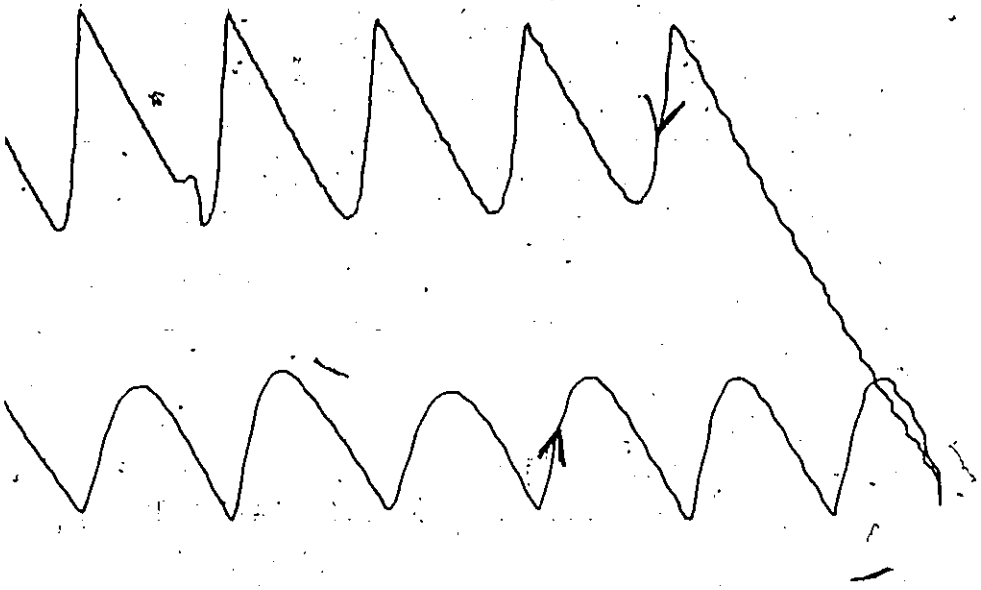

I_b = -0.26 A
B_a = Earth

Initial run

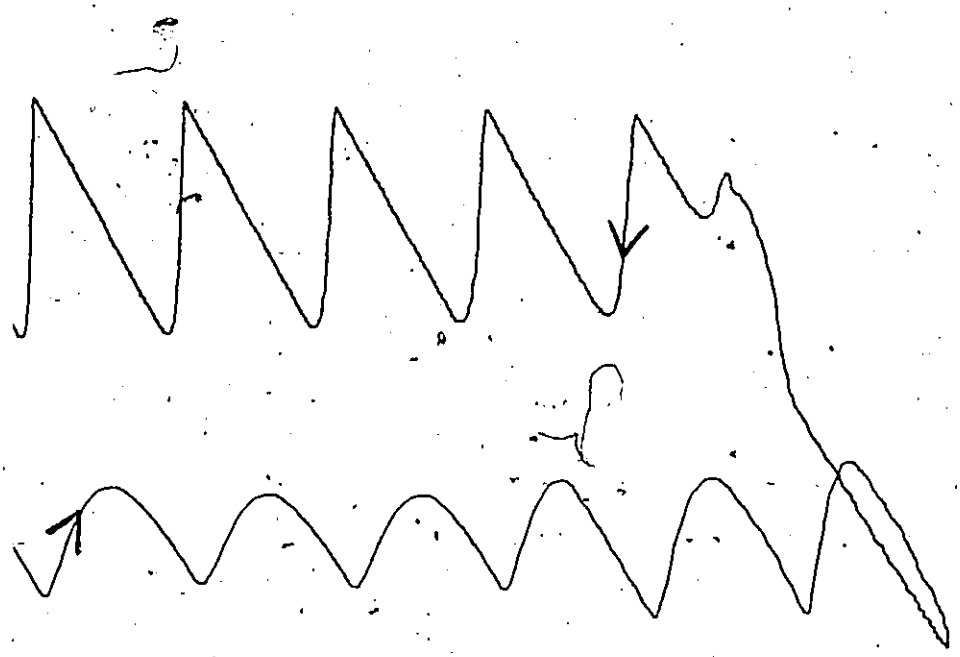

I_b = -0.26 A
B_a = Earth

Subsequent run

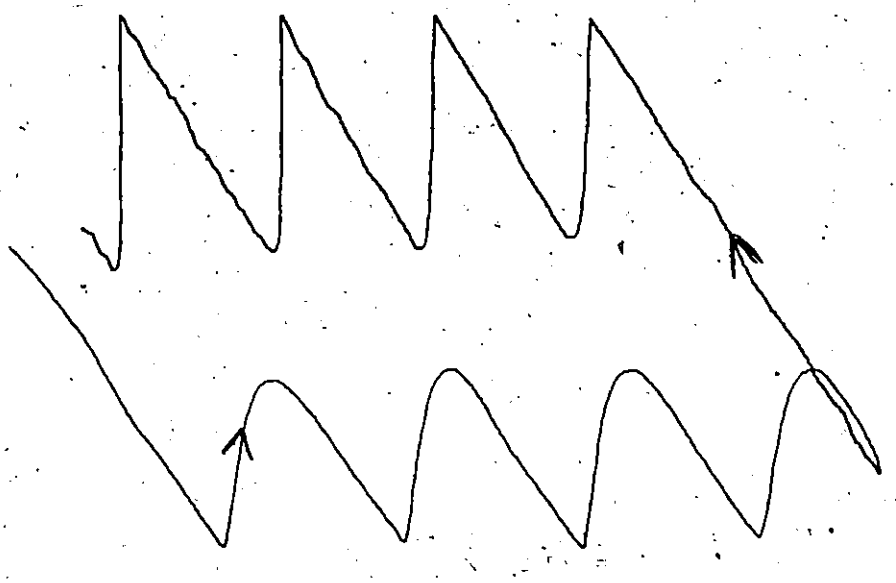

I_b = -0.26 A
B_a = Earth

Flux-flow voltage state

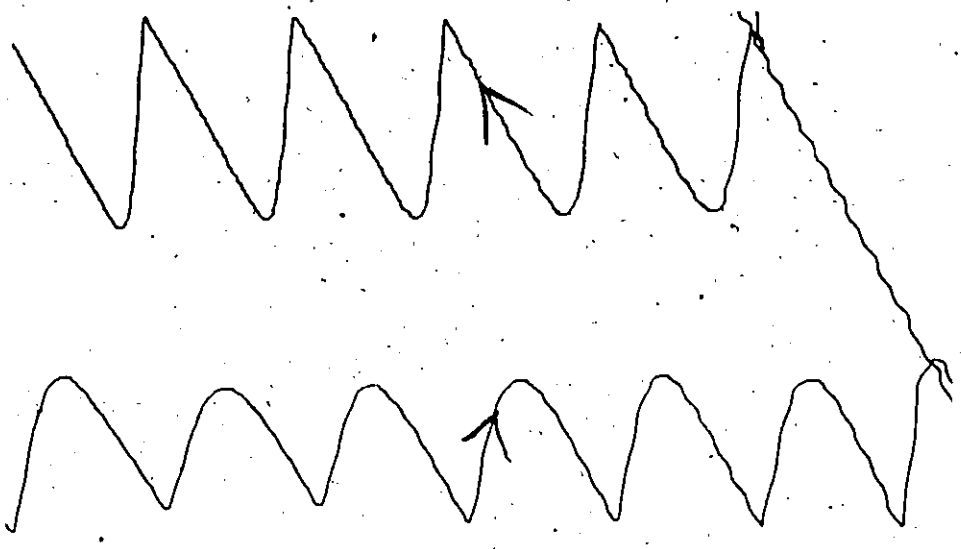

I_b = -0.26 A
B_a = 300 G

Initial run

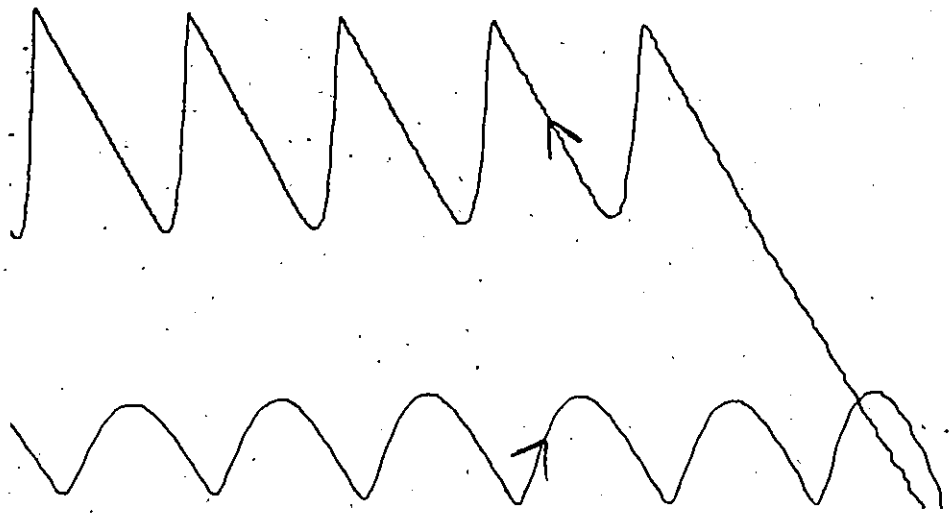

I_b = -0.26 A
B_a = 300 G

Subsequent run

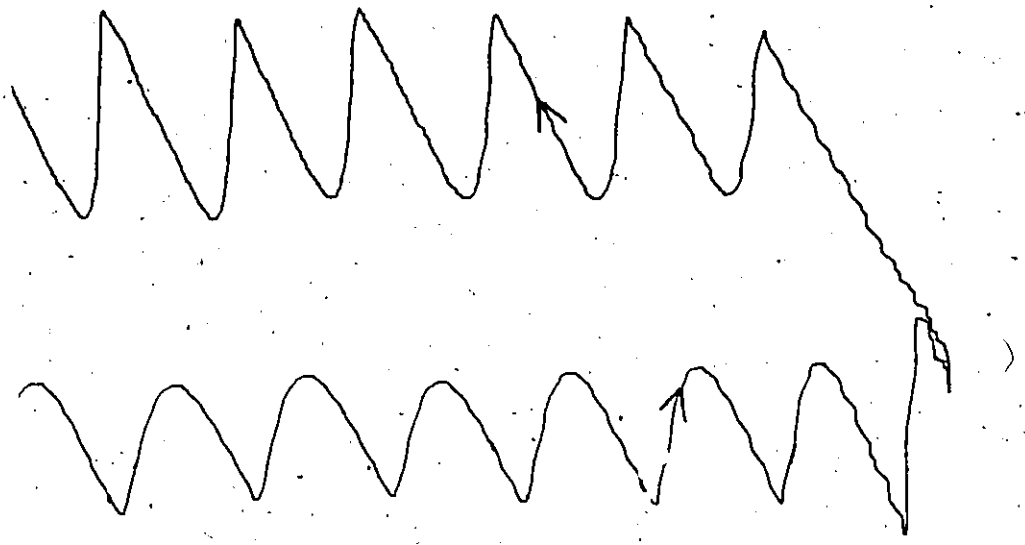

I_b = -0.26 A
B_a = 300 G

Flux-flow voltage state

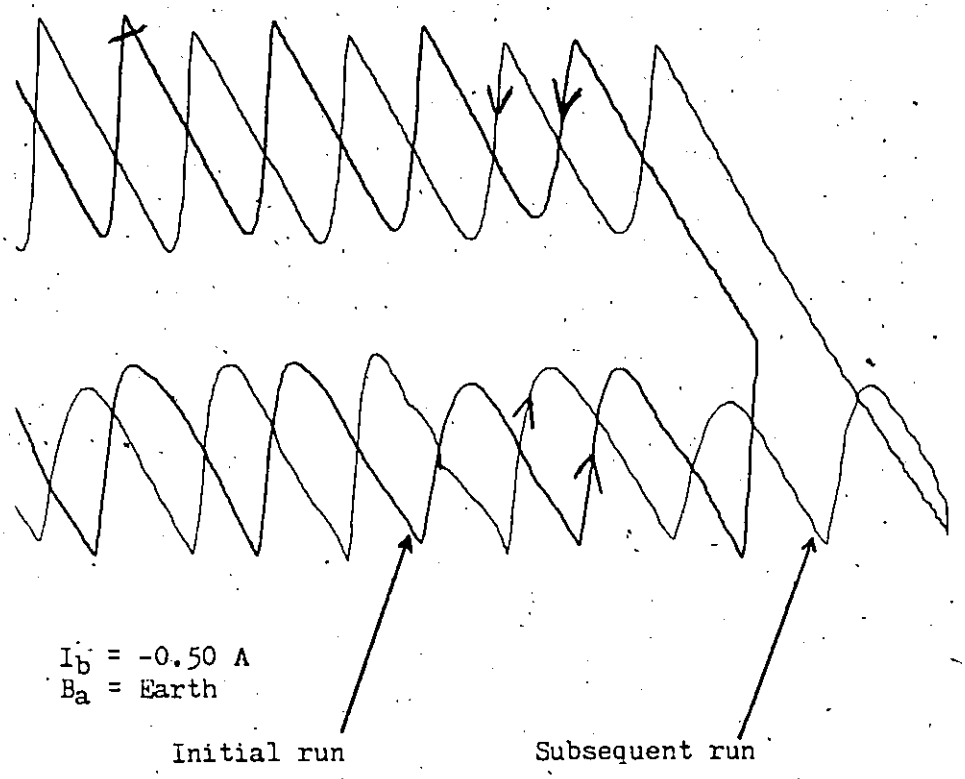
I_b = -0.50 A
B_a = Earth
Initial run
Subsequent run

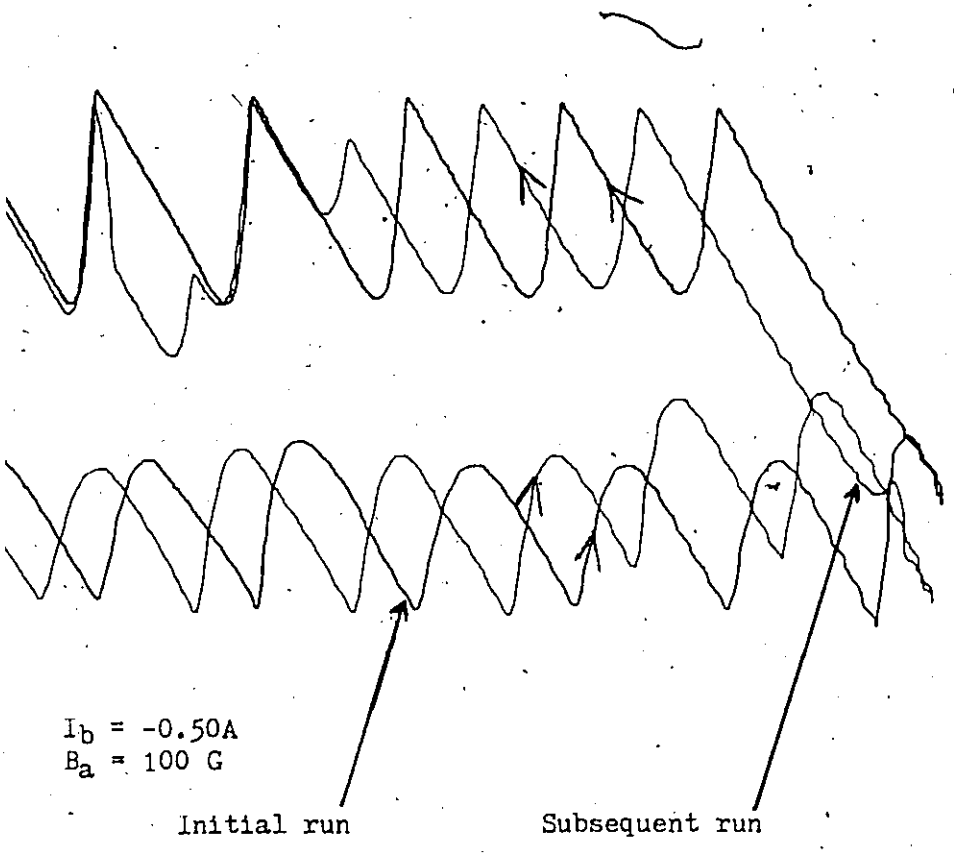
I_b = -0.50A
B_a = 100 G
Initial run
Subsequent run

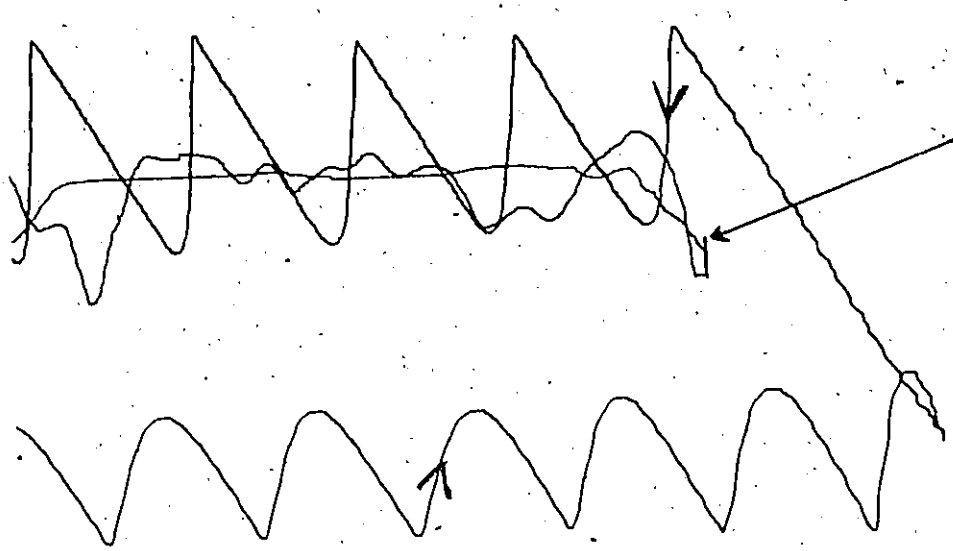

I_b = -0.50 A
B_a = 300 G

Initial run

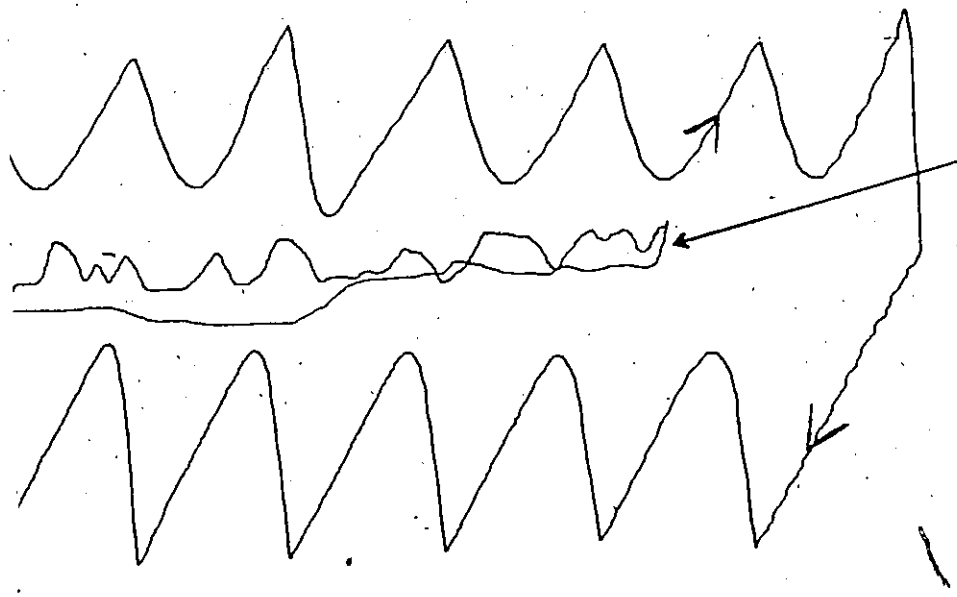

I_b = +0.50 A
B_a = Earth

Subsequent run

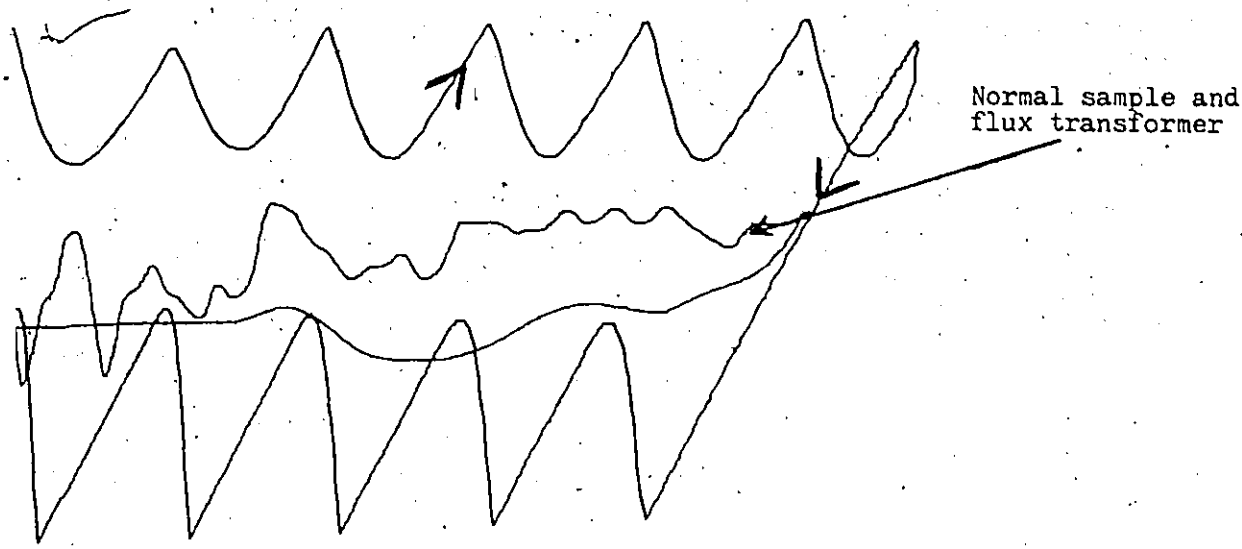

I_b = 40.50 A
B_a = 300 G

Initial run

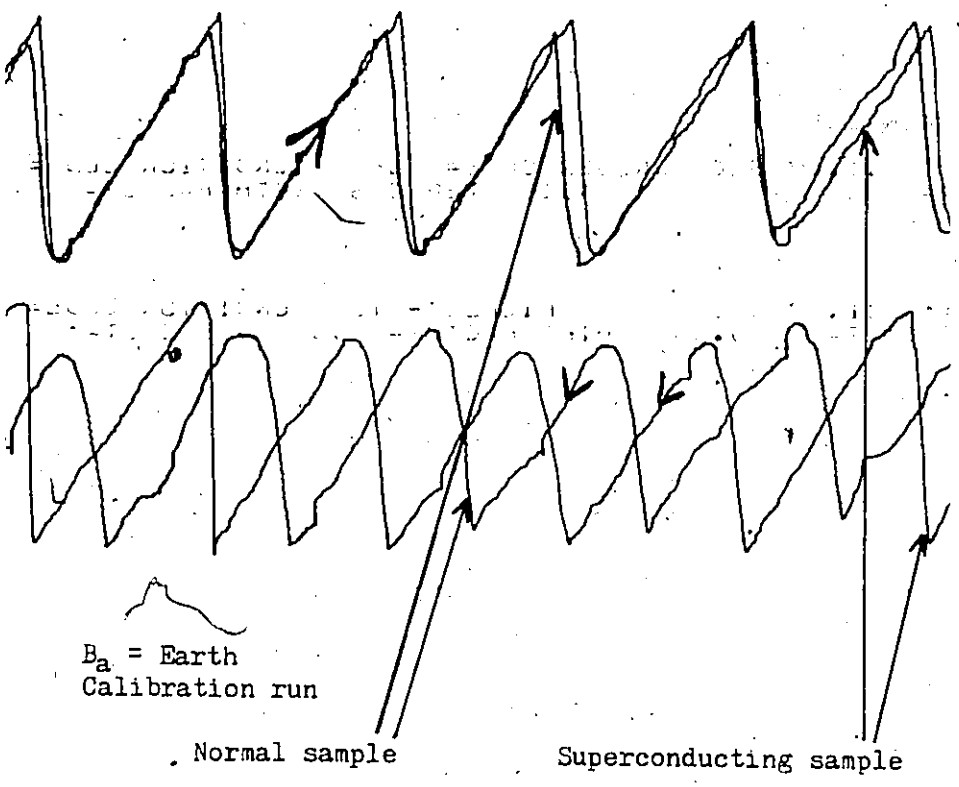

LIST OF REFERENCES

1. L. P. Gorkov, Soviet Phys. JETP 9, 1364 (1959).
2. R. G. Boyd, Phys. Rev. 145, 255 (1966).
3. W. Klose, Phys Letters 8, 12 (1964).
4. F. London and H. London, Proc. Roy. Soc. A149, 71 (1935).
5. A. B. Pippard, Physica 19, 765 (1953).
6. A. A. Abrikosov, Soviet Phys. JETP 5, 1174 (1957).
7. U. A. Rocher and J. C. Renard, Phys. Letters 25A, 119 (1967).
8. J. D. Cribier, B. Jacrot, L. Madhave Fao, and B. Farnoux, Progress in Low Temperature Physics, vol. V (North-Holland Publishing Company, Amsterdam, 1967) edited by C. J. Gorter.
9. A. G. Redfield, Phys. Rev. 162, 367 (1967).
10. A. H. Silver and J. E. Zimmerman, Phys. Rev. Letters 15, 888 (1965).
11. U. Essmann and H. Trauble, Phys. Letters 24A, 526 (1967).
12. D. G. Walmsley, J. Phys. F: Metal Phys. 2, 529 (1972).
13. M. A. R. LeBlanc, B. C. Belanger, and R. M. Fielding, Phys. Rev. Letters 14, 704 (1965).
14. D. G. Walmsley, J. Phys. F: Metal Phys. 2, 510 (1972).
15. P. W. Anderson and Y. B. Kim, Rev. Mod. Phys. 36, 39 (1964).
16. S. L. Wipf, Phys. Rev. 161, 404 (1967).
17. C. P. Bean, et al., Air Force Technical Report AFML-TR-65-431 (1966), Chapter 6.
18. D. Saint-James and P. G. deGennes, Phys. Letters 7, 306 (1963).
19. M. A. R. LeBlanc and H. G. Mattes, Solid State Comm. 4, 267 (1966).
20. D. G. Walmsley, J. Phys. F 2, 529 (1972).
21. M. A. R. LeBlanc, Phys. Rev. 143, 220 (1966).

22. J. E. Nicholson and P. T. Sikora, J. Low Temp. Phys. 17, 275 (1974).

23. B. D. Josephson, Phys. Letters 1, 251 (1962).

24. F. London, Superfluids 1, (1950).

25. B. S. Deaver, Jr. and W. M. Fairbank, Phys. Rev. Letters 7, 43 (1961).

26. R. Doll and M. Nabauer, Phys. Rev. Letters 7, 51 (1961).

27. J. Kurkijärvi, Phys. Rev. 36, 832 (1972).

28. Operating Instructions SHE Model 202, 7-5.

29. J. W. Thomasson and D. M. Ginsberg, Rev. Sci. Instrum 47, 387 (1976).

30. B. Cabrera, Ph.D. Thesis (1975).

31. J. C. Gallop and B. W. Petley, J. Phys. E: Sci. Instrum 9, 421 (1976).

32. G. Lamarche, private communication.